

Multi-scale soil moisture data and process-based modeling reveal the importance of lateral groundwater flow in a subarctic catchment

Jari-Pekka Nousu^{1,2}, Kersti Leppä², Hannu Marttila¹, Pertti Ala-aho¹, Giulia Mazzotti³, Terhikki Manninen⁴, Mika Korhonen⁵, Mika Aurela⁵, Annalea Lohila^{5,6}, and Samuli Launiainen²

¹Water, Energy and Environmental Engineering Research Unit, P.O. Box 4300, 90014 University of Oulu, Finland

²Bioeconomy and Environment, Natural Resources Institute Finland, Helsinki, Finland

³Univ. Grenoble Alpes, Université de Toulouse, Météo-France, CNRS, CNRM, Centre d'Études de la Neige, Grenoble, France

⁴Meteorological Research, Finnish Meteorological Institute, P.O. Box 503, 00101, Helsinki, Finland

⁵Climate System Research, Finnish Meteorological Institute, P.O. Box 503, 00101, Helsinki, Finland

⁶Institute for Atmospheric and Earth System Research INAR, University of Helsinki, Helsinki, Finland

Correspondence: Jari-Pekka Nousu (jari-pekka.nousu@luke.fi)

Abstract. Soil moisture plays a key role in soil nutrient and carbon cycling, plant productivity and in energy, water, and greenhouse gas exchanges between the land and the atmosphere. The knowledge on drivers of spatiotemporal soil moisture dynamics in subarctic landscape is limited. In this study, we used the Spatial Forest Hydrology (SpaFHy) model, *in-situ* soil moisture data and Sentinel-1 SAR-based soil moisture estimates to explore spatiotemporal controls of soil moisture in a subarctic headwater catchment in northwestern Finland. The role of groundwater dynamics and lateral flow on soil moisture was studied through three groundwater model conceptualizations: i) omission of groundwater storage and lateral flow, ii) conceptual TOPMODEL approach based on topographic wetness index, and iii) explicit 2D lateral groundwater flow. The model simulations were compared against continuous point soil moisture measurements, distributed manual measurements, and novel SAR-based soil moisture estimates available at high spatial and temporal resolution. Based on model scenarios and model-data comparison, we assessed when and where the lateral groundwater flow shapes shallow soil moisture, and under which conditions soil moisture variability is driven more by local ecohydrology, i.e. the balance of infiltration, drainage and evapotranspiration. The choice of groundwater flow model was shown to have a strong impact on modeled soil moisture dynamics within the catchment. All model conceptualizations captured the observed soil moisture dynamics in the upland forests, but accounting for the lateral groundwater flow was necessary to reproduce the saturated conditions common on the peatlands and occasionally on lowland forest grid-cells. We further highlight the potential of integrating multi-scale observations with land surface and hydrological models. The results have implications for ecohydrological and biogeochemical processes as well as modeling hydrology and Earth system feedbacks in subarctic and boreal environments.

1 Introduction

Soil moisture has a direct influence on land surface energy fluxes (Seneviratne et al., 2010; Ji et al., 2017), partitioning of precipitation into infiltration and runoff (Liu et al., 2019; Singh et al., 2021), and plant productivity and water use (Daly and

Porporato, 2005; Lagergren and Lindroth, 2002). It is also a key variable controlling soil microbial activity and consequent greenhouse gas emissions (Bonan, 1990; Karhu et al., 2014; Lohila et al., 2016; Makhnykina et al., 2020), and soil carbon balance (Larson et al., 2023). In the boreal and subarctic region, climate change is predicted to amplify seasonal variability of soil moisture due to longer and more frequent summer droughts, increased autumn and winter precipitation (Holmberg et al., 2014; Ruosteenoja et al., 2018), and changes in snow accumulation and melt (Räisänen, 2021). The altered soil moisture dynamics have an effect on the severity of abiotic stressors (e.g. water shortage, excess water, extreme temperatures) and biotic damages, affecting tree health, mortality and forest productivity (Buermann et al., 2014; Muukkonen et al., 2015; Wang et al., 2023). The changes in soil moisture across the landscape can significantly impact vegetation dynamics and alter competition between species, shaping the structures of the ecosystem (Venäläinen et al., 2020; Junttila et al., 2022; Ameray et al., 2023). Moreover, northern peatlands are sources of methane (Huttunen et al., 2003; Schneider et al., 2016) and boreal upland forests can turn from methane sinks to sources under long-lasting high soil moisture conditions (Korkiakoski et al., 2022; Lohila et al., 2016). Hence, accurate information on spatiotemporal soil moisture conditions has the potential to improve estimates of tree health, terrestrial carbon stocks and greenhouse gas sinks and sources, as well as lateral export of carbon and nutrients (Bond-Lamberty et al., 2016; Nakhavali et al., 2021). Soil moisture dynamics is also critical for weather and hydrological forecasting (Zhang et al., 2020a; Joo and Tian, 2021), climate change impact studies (Seneviratne et al., 2010; Kløve et al., 2014; IPCC, 2019), and for developing sustainable forest management practices (Salmivaara et al., 2021; Kankare et al., 2019).

Soil moisture has strong spatiotemporal variability driven by hydrometeorological conditions, landscape heterogeneity, and hydrological connectivity through lateral groundwater flow (Corradini, 2014; Kemppinen et al., 2023; Kim and Mohanty, 2016; Ji et al., 2017). The unsaturated soil is bounded at the bottom by the water table, and exchanges between the saturated and unsaturated zone occur through upward capillary rise and downward percolation (Maxwell et al., 2007; Miguez-Macho et al., 2007; J.-P. Vergnes and Habets, 2014). The lateral groundwater flow and consequent variation in the water table depth influences soil moisture especially in areas with shallow water table such as riparian areas, floodplains, and peatlands (Krinner, 2003; Decharme et al., 2019; Kollet and Maxwell, 2008).

Information on soil moisture dynamics can be obtained via *in-situ* measurements and remote sensing, as well as using numerical models (Robinson et al., 2008; Yu et al., 2021; Dobriyal et al., 2012). Continuous automatic *in-situ* measurements are well suited to capture soil moisture patterns at high temporal resolution at point-scale (Moreno et al., 2022; Kemppinen et al., 2023). However, distributing the observation network in space requires significant resources (Tyystjärvi et al., 2022) and is thus restricted to specific study areas (Kemppinen et al., 2023). Recent advances in satellite remote sensing have shown the potential to obtain soil moisture estimates at high spatial resolution (e.g. Sentinel-1 Synthetic Aperture Radar (SAR): Quast et al. (2023); Bauer-Marschallinger et al. (2019); Manninen et al. (2021)), but their accuracy for high-latitude forests is still limited (Celik et al., 2022). To predict soil moisture conditions under environmental change, process-based hydrological models are a prerequisite. However, their development also relies largely on observations (Panday and Huyakorn, 2004; Tyystjärvi et al., 2022), and it is widely accepted that the integration of *in-situ* measurements, remote sensing, and process-based modeling is the best avenue forward (Crow and Yilmaz, 2014; Sidle, 2021; De Lannoy et al., 2022). To yield accurate predictions, it is

55 essential that process-based models represent the most relevant local features and processes that affect soil moisture dynamics (Sidle, 2021; Ji et al., 2017; Kollet and Maxwell, 2008).

Due to the proliferation of geospatial data on land use, topography, vegetation, and soil characteristics, spatially distributed models can to an increasing extent incorporate spatial variability in their parameterizations, and extend point-scale simulations to scales relevant for practical applications (Launiainen et al., 2019; Ma et al., 2016; Clark et al., 2015; Maneta and Silverman, 60 2013). To model soil moisture at high spatial resolution, incorporating the effects of local soil texture and vegetation, as well as the conceptualization of subsurface water storage and lateral flow become important. Integrated surface-groundwater models can explicitly represent these interactions in 3D (Ala-aho et al., 2017a; Thornton et al., 2022; Autio et al., 2023), but are rarely used in ecosystem studies or large-scale applications due to their vast data needs and low computational efficiency. Attention towards groundwater dynamics is rather recent in land surface models used in climate, weather and hydrological 65 modeling communities (Decharme et al., 2019; Zeng et al., 2018; Li et al., 2022; Maxwell and Condon, 2016; Ji et al., 2017; Niu et al., 2014). In catchment hydrological models, the lateral movement of groundwater is also rarely explicitly described, and the groundwater dynamics are often based on conceptual approaches such as the use of topographic wetness index (TWI) (Beven and Kirkby, 1979) or grid-cell independent groundwater buckets (Bergström, 1992). These simplified approaches can efficiently link grid-cell and catchment water budgets and simulate sufficient discharge dynamics (Launiainen et al., 2019). 70 They can also accurately estimate soil moisture dynamics at locations, where water balance is mostly driven by local processes, i.e. infiltration, vertical water percolation and evapotranspiration (ET), rather than lateral flow and capillary rise (Tyystjärvi et al., 2022). However, once the impacts of lateral groundwater flow and a shallow water table become more pronounced, models neglecting these processes encounter obvious challenges to accurately simulate soil moisture dynamics (Kollet and Maxwell, 2008). Consequently, they often exhibit dry biases that directly affect simulations of soil evaporation and plant 75 transpiration (Maxwell and Condon, 2016).

Hydrological models are currently advancing towards incorporating more processes at higher spatial resolution (Sidle, 2021; Wood et al., 2011), but model calibration and evaluation are still largely based on point-scale observations of soil moisture, ET and stream discharge at catchment outlet (Ala-aho et al., 2017b; Launiainen et al., 2019), creating uncertainties for spatiotemporal simulations (Koch et al., 2018). The persistent lack of spatial observations of hydrological fluxes and water storages 80 (model state variables) prevents leveraging the full potential of distributed models and available data on landscape characteristics. Recent advances in remote sensing to produce spatially explicit data of precipitation (Yu et al., 2022; Skofronick-Jackson et al., 2017) and ET (Bhattarai and Wagle, 2021), canopy and soil water content (Manninen et al., 2021; Zhang and Zhou, 2015), snow cover (Meriö et al., 2023), and water table depth (Toca et al., 2023; Räsänen et al., 2022; Isoaho et al., 2023) open new opportunities to evaluate (Niu et al., 2021) and in some cases calibrate (Koch et al., 2018) spatially distributed models. 85 Such data are increasingly included in hydrological model-data assimilation (Li et al., 2023; Deschamps-Berger et al., 2022).

In this study, we assess the controls of soil moisture dynamics at the subarctic Pallas Lompolojängänoja headwater catchment in northern Finland. We combine analysis of multi-scale observations, including *in-situ* continuous and manual soil moisture measurements (Marttila et al., 2021; Aurela et al., 2015), SAR-based spatiotemporal estimates (Manninen et al., 2021), and process-based hydrological modeling. We use the Spatial Forest Hydrology model (SpaFH_y; Launiainen et al., 2019) at high

90 spatial resolution ($16 \times 16 \text{ m}^2$) with three alternative conceptualizations for groundwater storage and dynamics. We focus particularly on the influence of a shallow water table and lateral groundwater flow, as well as vegetation heterogeneity on spatiotemporal soil moisture dynamics through the following research questions:

1. Where does lateral groundwater flow affect the temporal variability of shallow soil moisture?
2. How does the role of lateral groundwater flow compare to the impact of vegetation heterogeneity in shaping soil moisture
95 patterns?
3. How do SAR-based soil moisture estimates compare with the models, and can they be useful in model evaluation?

To answer the research questions, we compare and contrast model predictions i) between model conceptualisations, ii) against point-scale soil moisture data, and iii) against SAR-based soil moisture estimates available from the study area.

2 Materials and methods

100 2.1 Study site

Our study area is located in the Pallas area ($67^{\circ}59'N$ $24^{\circ}13'E$) in northwestern Finland (Fig. 1B,C). Pallas has over 85 years of meteorological observations (Lohila et al., 2015), and the area has been recently set up as an interdisciplinary platform for atmospheric, ecological, and hydrological research. It includes multiple eddy covariance (EC) stations measuring surface-atmosphere energy and greenhouse gas fluxes, and both manual and automated ecohydrological monitoring over a range of
105 ecosystem types (Marttila et al., 2021). The climate in the area is characterized as subarctic. The long-term annual (1991–2020) mean temperature and mean annual precipitation at the Muonio weather station, located approximately 25 km west of Pallas, are -0.6°C and 532 mm, respectively (Jokinen et al., 2021). The proportion of precipitation falling as snow is approximately 42 % (Marttila et al., 2021), and the seasonal snow cover persists from about October until May (Aurela et al., 2015). Particularly, we consider the Lompolojängänoja catchment (hereafter LJO, Fig. 1A), which has the total area of circa 4.5 km^2 with elevations
110 varying between 268 m and 364 m a.s.l. Soils in the upland parts of the catchment are mainly gravely sand and sandy tills, and vegetation cover varies from coniferous forests to various types of mires such as open fens, treed mires, and paludified forests. Except for a few small roads and ditches, the area has had little human influence and can be considered mostly a pristine subarctic headwater catchment. Figure 1A gives an overview of the landscape and the main measurement locations in the LJO catchment.

115 EC flux data and the meteorological data used in this paper was collected from two stations located in the catchment of Lompolojängänoja (Fig. 1A). The forest site Kenttäröva (ICOS Ecosystem associate site) is a Norway spruce-dominated forest growing on podzol soil with the age of the trees varying from 90 to 250 years. The number of trees, 643 and 68 stems ha^{-1} for spruce and deciduous trees (mainly *Betula pubescens*), has stayed the same since a survey in 2011 (Aurela et al., 2015). The dominant tree height is currently about 15.5 m and 11 m for spruce and *Betula pubescens*, respectively. In 2011, a mean

120 one-sided leaf-area index (LAI) for Norway spruce and *Betula pubescens* was 2.0 and 0.1 m² m⁻², respectively (Aurela et al., 2015).

The mire site Lompolojännkä (ICOS Ecosystem Class 2 site) is an open, mesotrophic sedge fen (Zhang et al., 2020b) with a maximum peat thickness of about 2.5 m (Mathijssen et al., 2014). The Lompolonjängänoja stream flows through the long and narrow fen, draining into a nearby lake Pallasjärvi. The dominant vascular species are *Andromeda polifolia*, *Betula nana* and
125 *B. pubescens*, *Carex spp.*, *Equisetum spp.*, *Eriophorum spp.* The dominant moss species are *Sphagnum spp.*, whose coverage is about 50 %. The mean one-sided LAI was 1.4 m² m⁻² and the mean vegetation height 0.4 m in 2018.

2.2 Models

We used the Spatial Forest Hydrology model (SpaFHy; Launiainen et al., 2019), developed to predict spatial and temporal patterns of hydrological fluxes and state variables in the vegetation canopy, organic moss-humus layer, and in top soil (rootzone).
130 SpaFHy has been tested for 9 EC-flux sites in Finland and Sweden (stand-scale; ET and soil moisture) and for 21 small boreal headwater catchments in Finland (catchment-scale; runoff dynamics and ET to precipitation ratio) in Launiainen et al. (2019). It has been adapted to drained peatland forests (Leppä et al., 2020; Stenberg et al., 2022), extended with nutrient balance and leaching modules (Laurén et al., 2021), applied to model forest drought risks (Launiainen et al., 2022) and used to predict soil moisture dynamics in the arctic tundra (Tyystjärvi et al., 2022). Its aim is to provide a simple and practically applicable
135 framework to study the effects of landscape heterogeneity, management and macroclimatic change on catchment hydrology in boreal and subarctic landscapes.

The original SpaFHy includes two groundwater conceptualizations: a free drainage approach (i.e. neglecting groundwater dynamics, SpaFHy-1D) and a TOPMODEL-based approach (i.e. groundwater return flow based on topographic wetness index, SpaFHy-TOP). In this study, we implemented a new submodel to represent the 2D lateral Darcy flow (SpaFHy-2D). The salient
140 features of the three model versions are briefly described next and summarized in Table 1. The general model parameters are given in Table 2.

2.2.1 SpaFHy-1D

SpaFHy-1D considers grid-cells as independent hydrological units (Launiainen et al., 2019). The hydrological processes in the vegetation canopy, snowpack, organic moss-humus layer, and rootzone are explicitly simulated at a daily timestep for each
145 grid-cell in the model domain. The above-ground fluxes and state variables are computed in the canopy submodel, including rainfall and snowfall interception and evaporation, throughfall, transpiration, and snow accumulation and snowmelt (see Sect. 2.2. in Launiainen et al. (2019)). Snowmelt is computed with a degree-day approach while ET components are solved by the Penman–Monteith equation. For transpiration, the canopy conductance is derived from the stomatal optimality principle and accounting for an exponential attenuation of light in the canopy (Launiainen et al., 2019). The bucket submodel describes
150 top soil hydrology and soil moisture dynamics in two layers. The upper layer is the organic moss-humus layer, whose water budget is affected by throughfall and snowmelt interception and soil evaporation, as well as infiltration to the lower rootzone layer, where drainage and transpiration take place. The lateral water flow between the grid-cells is omitted, and drainage from

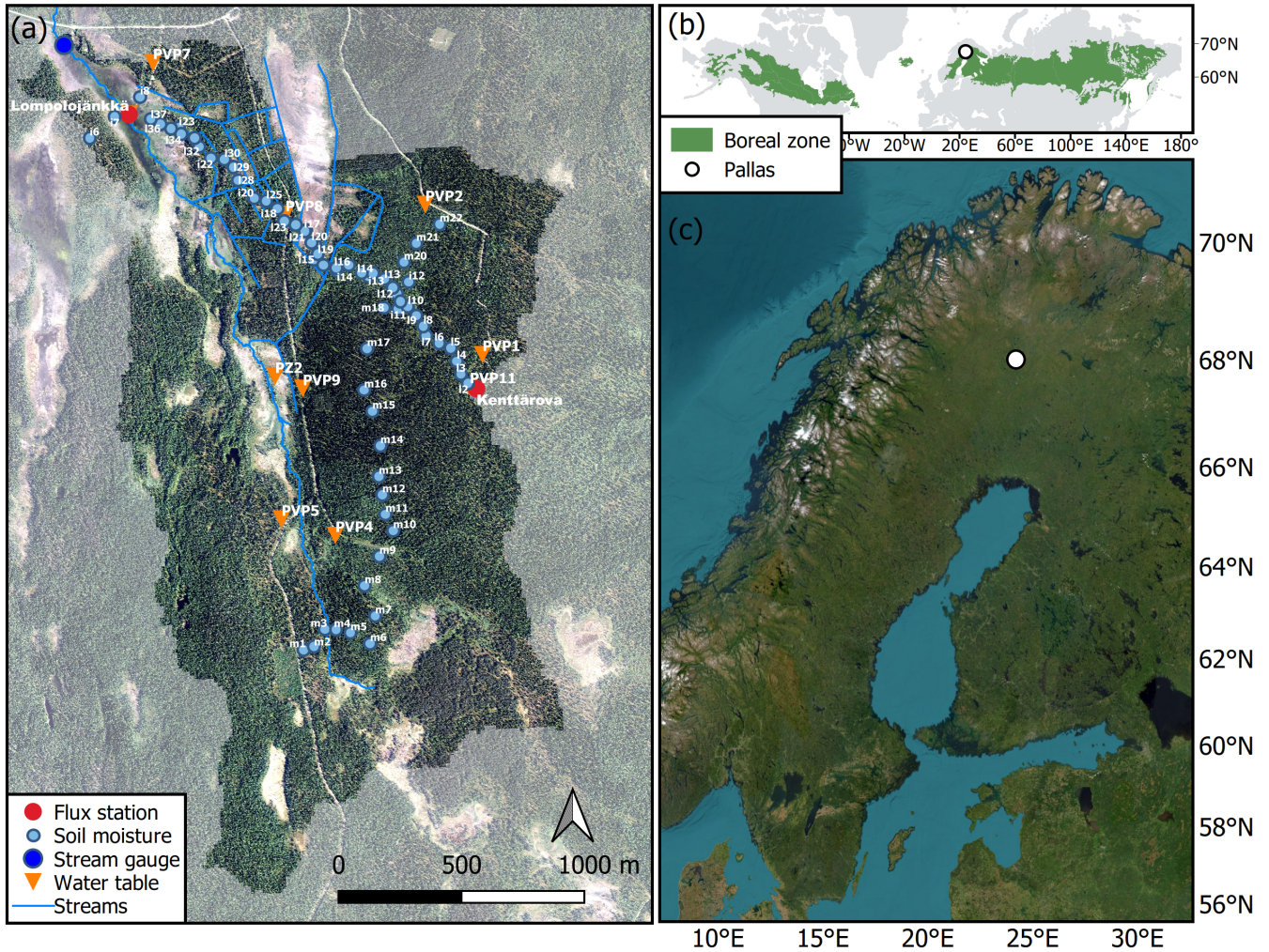


Figure 1. The Lompolojängänoja (LJO) catchment and its hydrological measurement locations (A, the aerial image by NLSF, 2020) is located in the northern boreal zone (B, green area, Olson et al., 2001) in northwestern Finland (C, Esri, 2023). The ICOS flux stations Kenttäröva (forest) and Lompolonjängkä (open mire) are presented in red circles, stream gauge in blue, soil moisture measurement locations are labeled and presented in light blue, and water table depth monitoring locations are labeled and presented in orange. Streams are shown as blue lines.

the bucket submodel is removed from the model domain as stream discharge at the catchment outlet without a delay. Thus, SpaFHy-1D represents a situation where soil moisture variability within the catchment is driven solely by the heterogeneity of vegetation, soil characteristics, and meteorological forcing. Similar conceptualizations of soil hydrology are common for large-scale land surface and hydrological models (Smith et al., 2001; Seibert and Vis, 2012; Clark et al., 2008; Niu et al., 2011). The canopy and bucket submodels are common to all three SpaFHy versions.

2.2.2 SpaFHy-TOP

SpaFHy-TOP includes a conceptual description of the saturated zone using the TOPMODEL approach (Beven and Kirkby, 1979). Drainage from the bucket submodel feeds TOPMODEL's lumped catchment groundwater storage, which is then spatially distributed via the topographic wetness index (TWI). The TWI is defined as the natural logarithm of the flow accumulation area (i.e. upslope area draining through the grid-cell) divided by the tangent of the local slope (Beven and Kirkby, 1979). The local saturation deficit is related to the TWI and catchment average saturation deficit, creating a higher probability for grid-cells with greater TWI to become saturated. During a model timestep, return flow from groundwater storage to rootzone and organic moss-humus layer occurs in grid-cells where local saturation deficit is zero (Launiainen et al., 2019). The return flow is routed through rootzone and the organic moss-humus layer and their respective soil moisture updated, while potential excess water becomes surface runoff. Discharge at the catchment outlet is the sum of catchment average baseflow (predicted by TOPMODEL) and surface runoff without a delay. This version of SpaFHy-TOP is identical to the one used in Launiainen et al. (2019, 2022).

2.2.3 SpaFHy-2D

SpaFHy-2D version was developed in this study to explicitly describe lateral groundwater flow within the catchment. The modeling domain consists of soil columns whose relative elevation to one another is defined by the digital elevation model. Each soil column extends to an impermeable layer (no-flow boundary) at a predefined depth, while the columns are characterized by their water retention characteristics (following the van Genuchten -model; van Genuchten, 1980) and saturated hydraulic conductivity based on the soil type.

Lateral flow in the saturated zone is solved using the 2D groundwater flow equation:

$$C \frac{\partial h}{\partial t} = \frac{\partial h}{\partial x} \left(T \frac{\partial h}{\partial x} \right) + \frac{\partial h}{\partial y} \left(T \frac{\partial h}{\partial y} \right) + S \quad (1)$$

where t is time (d), x and y are the horizontal dimensions (m), C is the storage coefficient (m m^{-1}), T is transmissivity ($\text{m}^2 \text{d}^{-1}$), h is the hydraulic head (m), and S (m d^{-1}) is water drained from the overlaying bucket submodel. Lateral groundwater flow between grid-cells takes place only in the saturated zone, and thus T is obtained by integrating the saturated hydraulic conductivity over the saturated layer depth. C describes the change in h relative to a change in the soil column water content W (m). The relation between h and W is solved based on the assumption that in the unsaturated zone the water content profile sets to hydraulic equilibrium (constant hydraulic head in vertical dimension; Skaggs, 1980). For numerical efficiency of solving Eq. 1, interpolation functions for $W(h)$, $T(h)$, and $C(h)$ were constructed prior to simulation for each soil column type (Laurén

et al., 2021). When the soil column becomes oversaturated, i.e. groundwater level rises to rootzone, the excess water is routed
185 as return flow to the bucket submodel, similarly as in SpaFHy-TOP.

Streams (and ditches) in the catchment were described as grid-cells with constant h . The outflow to streams is computed
from the local hydraulic head gradient when the surrounding water table level is above the stream h . No flow from stream to
soil is allowed. We do not consider temporal changes in stream water level and omit channel flow in the stream network; thus
the sum of the outflow into the stream cells and surface runoff form the runoff at the catchment outlet without a delay. The
190 assumption of a constant stream water level simplifies the modeling framework and should not significantly impact catchment
soil moisture dynamics. Catchment borders are defined as no flow boundaries, assuming no significant water flows occur
between the delineated catchment and its surroundings that impact shallow soil moisture.

2.3 Model input

2.3.1 Geospatial data

195 To set up SpaFHy for the LJO catchment, we used mainly open geospatial data that is available throughout Finland. The rasters
used are presented in Fig. 2, and summarized in Table 1.

For canopy attributes and for distinguishing between forest soils and mires, we used the multi-source National Forest In-
ventory (mNFI; Mäkisara et al., 2016) data at 16 m horizontal resolution. This was also chosen as the model grid resolution
for the simulations, and other input rasters were aggregated accordingly, consistent with Launiainen et al. (2019). From mNFI
200 data, needle and leaf mass rasters were used to derive one-sided LAI of deciduous and coniferous trees. LAI values were esti-
mated using specific one-sided leaf areas for pine, spruce and birch (6.8, 4.7 and 12.0 m² kg⁻¹, respectively; Härkönen et al.,
2015). LAI estimates of shrub and grass were adopted from local multi-source remote sensing data by Räsänen et al. (2021).
The canopy fraction and prevailing site class (used for parameterizing organic moss-humus layer) were also obtained from the
mNFI data.

205 The soil type affects hydraulic properties of the rootzone and the SpaFHy-2D lateral groundwater flow module. A combined
soil type raster was constructed by taking the peatland boundaries from the National Land Survey of Finland topographic
map NLSF (2020) and the remaining soil characteristics from the Geological Survey of Finland soil texture map (GSF, 2020)
similarly to Launiainen et al. (2019).

The catchment was delineated based on the digital elevation model (NLSF, 2020) with Whitebox GAT software (Lindsay,
210 2014). TWI was calculated using the slope and flow accumulation raster, with the flow accumulation determined through the
D8 method (O'Callaghan and Mark, 1984). The stream network was obtained from NLSF (2020). Furthermore, topographic
impacts for solar radiation were considered by computing a daily shading coefficient, calculated as the potential daily radiation
input for each grid-cell normalized by the potential input at the grid-cell of the Kenttäröva station, where the global radiation
forcing was measured (see Sect. 2.3.2).

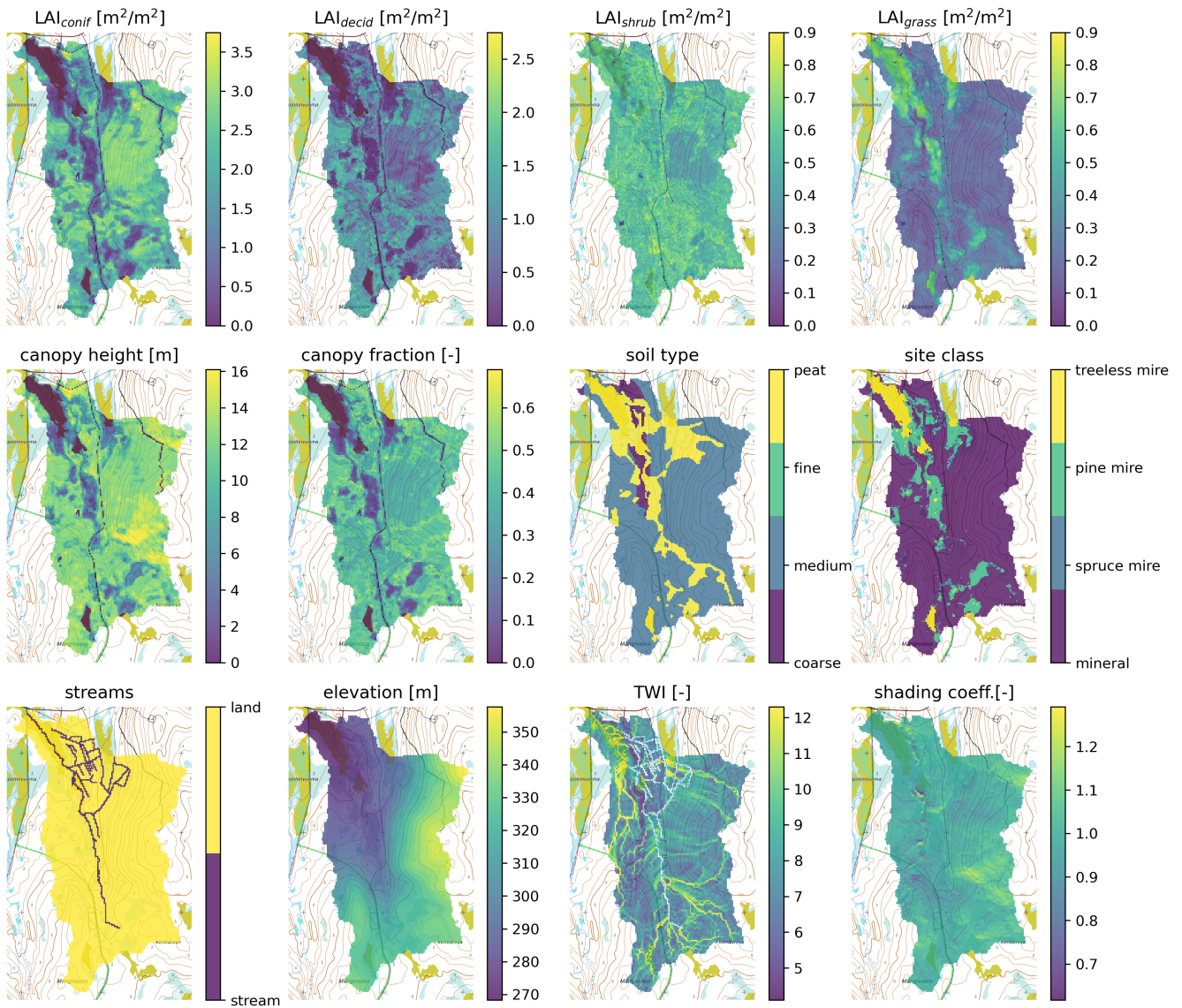


Figure 2. Set of geospatial rasters used to set up the model for the LJO catchment. Top row shows leaf-area index (LAI) for different plant types. For each grid-cell, the conifer and deciduous LAI forms the canopy LAI, and understory LAI is the sum of shrubs and grasses. TWI is the topographic wetness index. The rasters overlay a topographic map (NLSF, 2020).

Table 1. Geospatial data used by each submodel, and submodel used by each model configuration.

Geospatial data	Canopy	Bucket	TOPMODEL	2D Flow
Digital elevation model			✓	✓
Catchment mask	✓	✓	✓	✓
Topographic wetness index			✓	
Shading coefficient	✓	✓		
Site class		✓		
Leaf area index	✓			
Canopy height	✓			
Canopy fraction	✓			
Soil type		✓		✓
Streams				✓
Model configuration	Canopy	Bucket	TOPMODEL	2D Flow
1D	✓	✓		
TOP	✓	✓	✓	
2D	✓	✓		✓

215 2.3.2 Meteorological forcing

All SpaFH_y versions require the same daily meteorological forcing: mean air temperature T_a ($^{\circ}\text{C}$), global radiation R_g (Wm^{-2}), relative humidity RH (%), wind speed U (m^{-1}) and daily accumulated precipitation P (mm). This data was compiled and made available by Nousu et al. (2023), and includes *in-situ* observations at Kenttäröva station available from the Finnish Meteorological Institute (FMI) open database (FMI, 2021), supplemented by FMI’s R_g observations from the Kenttäröva station (located at the hilltop, Fig. 1). The data gaps in R_g were first filled by data from contiguous sites and then by ERA5 reanalysis data (Hersbach et al., 2020). We multiplied the R_g forcing by the shading coefficient (see Sect. 2.3.1) for each day (Fig. 2) to account for the topographic effects on the radiation forcing at each grid cell. For the other meteorological variables, a spatially uniform forcing was applied.

2.4 Model parameterization

225 The canopy and bucket submodels were common to all model versions and parameterized as in Launiainen et al. (2019). The only exception was the organic moss-humus layer, which was refined to allow for full or partial saturation in situations where upward return flow occurs from the rootzone layer. Drainage from the organic moss-humus layer to the rootzone layer is represented identically as the drainage from the rootzone layer (Eq. 18 in Launiainen et al. (2019)). A depth of 0.05 m was assigned to the organic moss-humus layer (Table 2). To account for the different hydraulic properties of the organic

230 moss-humus layer in mineral forest soils (dominated by feather mosses) and peatlands (mainly Sphagnum moss), the moss hydraulic parameters (porosity, field capacity, and relative available water) were derived from Williams and Flanagan (1996) and Elumeeva et al. (2011). The peatlands and mineral soils were separated based on mNFI site class (see Fig. 2); the site class and soil type -specific parameters for the organic moss-humus, rootzone and deep soil layers are given in the Supplement (Table S1–S3). Available literature was used to define the van Genuchten (1980) water retention parameters for the Bucket and 2D Flow submodels (Autio et al., 2023; Menberu et al., 2021). The rootzone was assigned a depth of 0.30 m (Table 2). Due to a lack of reliable data on the depth-to-bedrock, a uniform thickness of 5 m was assigned for the deep soil layer of the 2D groundwater module throughout the model domain. This estimate corresponds approximately to the thickest peat layers and the shallowest mineral soil depths of the catchment (Autio et al., 2023). Canopy parameters for surface conductance for evaporation from the wet forest floor (G_f) and canopy storage capacity for rain (w_{max}), and the TOPMODEL effective soil depth parameter were obtained from Launiainen et al. (2019). No further calibration or sensitivity tests of any model parameters were conducted in this study.

Model simulations with the three different treatments of groundwater dynamics (named 1D, TOP and 2D) were run with identical meteorological forcing, geospatial inputs (Fig. 2), and canopy and bucket submodel parameterizations (Table 2). To study how spatially heterogeneous vegetation affects soil moisture, additional 1D simulation was run with site class specific mean vegetation parameters. This experiment is referred to as 1D_{homog.canopy}, and vegetation characteristics at each grid-cell belonging to a certain site class (Fig. 2) were set to the average of that particular site class (see Fig. S1). All simulations cover period from 2011-01-01 to 2021-09-01, of which the beginning until 2013-09-01 was considered as a model spin-up period and omitted from subsequent analysis.

2.5 Hydrological observations

250 This study benefits from the extensive hydrological monitoring of the LJO catchment (Marttila et al., 2021; Aurela et al., 2015). We further conducted several campaigns to measure spatiotemporal variability of soil moisture (i.e. volumetric water content θ) during 2019–2021. In particular, during snow-free seasons, biweekly manual measurements at 15 different points (denoted as "i" in Fig. 1) were conducted using WET-2 and PR2 Profile Probe sensors with an HH2 readout unit (Delta-T Devices Ltd., Cambridge, U.K.) sampling soil moisture profile at depths 0 cm, 10 cm, 20 cm and 30 cm (from the soil surface). Additionally, we conducted two extended soil moisture measurement campaigns, including 56 additional locations (denoted as "l" and "m" in Fig. 1). The first (2021-06-17) represents wet condition when soil moisture was still highly impacted by the snowmelt. The second (2021-09-01) was conducted in early autumn conditions after a precipitation event. Both these campaigns used the sensor ML3 ThetaProbe (Delta-T Devices Ltd., Cambridge U.K.) that measures soil moisture at 5 cm depth. For the ML3 ThetaProbe sensor, soil moisture at locations with peat soils at full saturation were assigned directly to the assumed peat porosity (0.89).

In addition, we used data from continuous soil moisture sensors distributed in close proximity to the Kenttäröva flux site. From 2013 to 2017, soil moisture was continuously measured by four ThetaProbe type ML2x sensors at 5 cm and 20 cm depths (two each) (Aurela et al., 2015). In 2017, more sensors were installed alongside the existing ones, among which we

used two sensors (Soil Scout Oy, Helsinki, Finland) at depths 5 cm and 30 cm (from the soil surface). The continuous soil
265 moisture measurements were averaged into daily values. To overcome the inherent uncertainties in *in-situ* measurements of
soil moisture, stemming from different devices and measurement and installation procedures (Robinson et al., 2008; Dobriyal
et al., 2012; Iwata et al., 2017), we present the means and variability ranges of continuous soil moisture sensors, and address
these uncertainties by averaging multiple manual probings within the area of interest within approximately a 5 m radius. All
soil moisture measurements from 0 to 30 cm depth correspond to the rootzone layer of SpaFHy. As soil moisture of the organic
270 moss-humus layer was not directly measured, we assume soil moisture measurements at the soil surface (0 cm depth) to best
represent this layer.

ET was measured by the eddy covariance (EC) technique at the two flux stations, Kenttäröva spruce forest and Lompolo-
jänkki peatland (Fig. 1A). The EC systems consist of USA-1 (METEK) 3D sonic anemometer and closed-path LI-7000 (Li-cor,
Inc.) CO₂/H₂O analysers (Aurela et al., 2015). EC data processing is described in detail in Aurela et al. (2015) and in Nousu
275 et al. (2023).

The runoff was measured by the Finnish Environment Institute with a 120-degree V-notch weir at the outlet (stream gauge in
Fig. 1A). Snow data consisted of automated snow depth observations at the Kenttäröva flux station, and approximately monthly
manual snow water equivalent (SWE) measurements at Kenttäröva and Lompolojänkki stations (Marttila et al., 2021).

2.6 SAR-based soil moisture estimates

280 We used SAR-based surface soil moisture estimates from the study area. This newly derived research data set was developed
by Manninen et al. (2021), who used Sentinel-1 Synthetic Aperture Radar (SAR) ground range detected high-resolution data
to produce high-resolution spatiotemporal soil moisture estimates. The soil moisture retrieval using SAR images is based
on the gradient boosting method, utilizing input variables of nonlocally averaged VH and VV backscattering coefficients,
multitemporal SAR statistics, terrain data, effective LAI estimates based on SAR, SAR overpass information, and the time for
285 the soil moisture estimate to be calculated. Distinct algorithms were developed for morning and evening flyovers, both relating
soil moisture estimates to instantaneous midday. They were validated against discrete and continuous *in-situ* soil moisture
measurements at Pallas (Manninen et al., 2021). In particular, the gradient boosted trees methods were trained with manual
surface soil moisture measurements (depth = 0 cm) and continuous soil moisture measurements at deeper soil layers that were
converted to surface conditions via linear regression in order to correspond to the penetration depth of the C-band SAR signal
290 in soil, which is in the range of 1–5 cm (Beale et al., 2021; Nolan and Fatland, 2003). Further details on the SAR data can be
found in Manninen et al. (2021). In this study, the original irregular grids with approximately 10 m pixel spacing were averaged
into a 16 m regular grid using subpixel area weights to be compared with the model outputs.

2.7 Evaluation methods

Annual periods are defined as hydrological years starting from September (e.g., 2016 = 2015-09-01 to 2016-08-31). We use
295 performance metrics of mean absolute error (MAE), mean bias error (MBE) and coefficient of determination (R^2) for model-
data comparison. Moreover, we use the Kling-Gupta Efficiency (KGE) (Gupta et al., 2009) for comparing daily runoffs between

Table 2. Parameters used by each submodel. Soil type- and site type-specific parameters are listed in the Supplement (Tables S1-S3).

Parameter	Value	Units	Explanation	Note
Canopy				
A_{max}	10	$\mu\text{mol m}^{-2} \text{s}^{-1}$	maximum leaf net assimilation rate	Launiainen et al. (2019)
$g_{1,c}$	2.1	$\text{kPa}^{0.5}$	stomatal parameter for conifers	Launiainen et al. (2015)
$g_{1,d}$	3.5	$\text{kPa}^{0.5}$	stomatal parameter for deciduous	Lin et al. (2015)
b	50	Wm^{-2}	half-saturation PAR of light response	Launiainen et al. (2019)
k_p	0.6	-	radiation attenuation coefficient	Launiainen et al. (2019)
r_w	0.2	-	critical relative extractable water	Lagergren and Lindroth (2002)
$r_{w,min}$	0.02	-	minimum relative conductance	Launiainen et al. (2019)
G_f	0.01	ms^{-1}	surface conductance for evaporation from wet forest floor	Launiainen et al. (2019)
w_{max}	1.5	mm LAI^{-1}	canopy storage capacity for rain	Launiainen et al. (2019)
$w_{max,snow}$	4.5	mm LAI^{-1}	canopy storage capacity for snow	Pomeroy et al. (1998), Essery et al. (2003)
K_m	2.5	mm d^{-1}	melt coefficient in open area	Kuusisto (1984)
K_f	0.5	mm d^{-1}	freezing coefficient	Koivusalo and Kokkonen (2002)
Y_{max}	18.5	$^{\circ}\text{C}$	phenology model parameter	Kolari et al. (2007)
τ	13	d	time constant	Kolari et al. (2007)
$T_{0,y}$	-4	$^{\circ}\text{C}$	base temperature	Kolari et al. (2007)
Bucket				
$z_{s,org}$	0.05	m	organic layer depth	Launiainen et al. (2019)
$z_{s,root}$	0.3	m	root zone depth	Kalliokoski et al. (2010)
TOPMODEL				
T_0	0.001	m s^{-1}	transmissivity at saturation	Launiainen et al. (2019)
m	0.05	m	effective soil depth	Launiainen et al. (2019)
2D Flow				
$z_{s,deep}$	5	m	deep soil layer thickness	assigned
z_{stream}	-0.2	m	stream water level relative to surface elevation	assigned

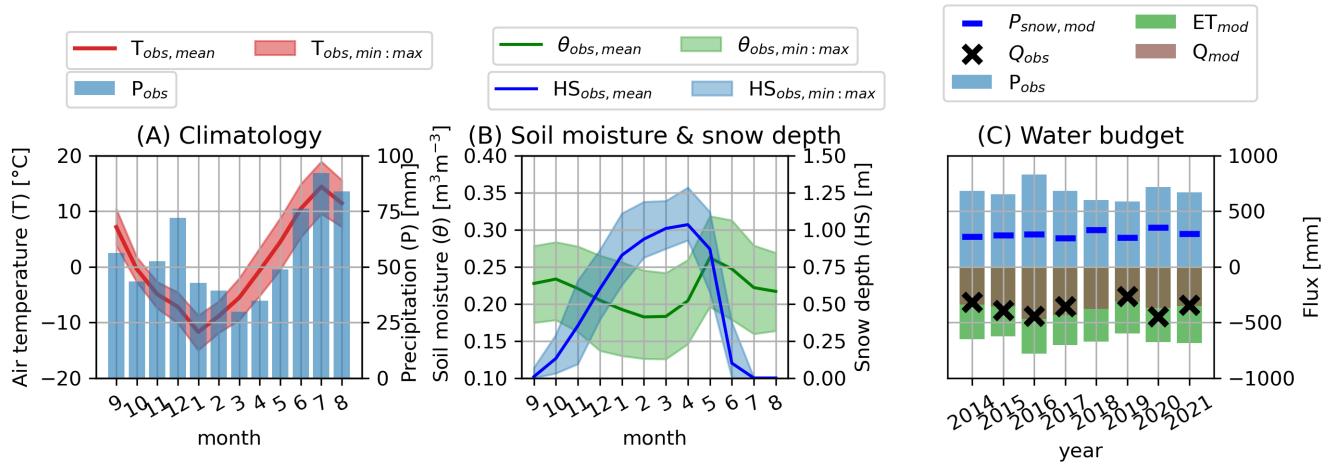


Figure 3. Hydrometeorological characteristics of Pallas. (A) Monthly observed climatology for the simulation period, (B) monthly observed volumetric soil moisture (θ) and snow depth (HS) at Kenttäröva forest site. The air temperature (T) and θ envelopes represent minimum and maximum monthly averages during simulation period, while the snow depth envelope shows minimum and maximum of monthly maximum during simulation period. (C) Annual water budget as observed (obs) and simulated (mod) with SpaFHy-2D, where Q is catchment runoff, ET evapotranspiration, P_{obs} is observed precipitation, and $P_{snow,mod}$ is modeled snow precipitation. The change in catchment water storage (including canopy water, soil water and groundwater storage) $dS/dt = P + ET + Q$ is not shown. Due to gaps in measurements, Q_{obs} is not available for 2018.

simulations and observations. Mean differences (MD) are computed to compare different simulations (i.e. the mean difference at each grid-cell).

3 Results

300 3.1 Climatology and water budget dynamics

As typical for high-latitudes, the period with permanent snow cover and freezing temperatures is long (Fig. 3A,B), with nearly half of the annual precipitation falling as snow (250 mm – 350 mm, Fig. 3C), resulting in annual peak snow depths from approximately 0.9 to 1.3 m (Fig. 3B). The snowmelt period commonly spans roughly from late April to the beginning of June, resulting in the highest soil moisture during snowmelt (Fig. 3B). The summer is characterized by cool to warm temperatures and higher precipitation that typically peaks in July (Fig. 3A).
305

Due to energy limitations for annual ET and large peak SWE, runoff dominates the water balance covering 49 to 67% of annual precipitation, while ET represents 34 to 50% depending on the year (Fig. 3C). SpaFHy-2D is able to closely capture the observed annual runoff during the simulated years (Fig. 3C). Also daily runoff dynamics are reasonably well represented by both SpaFHy-TOP (KGE: 0.63) and SpaFHy-2D (KGE: 0.65, see Fig. S2). The summer runoff dynamics after precipitation

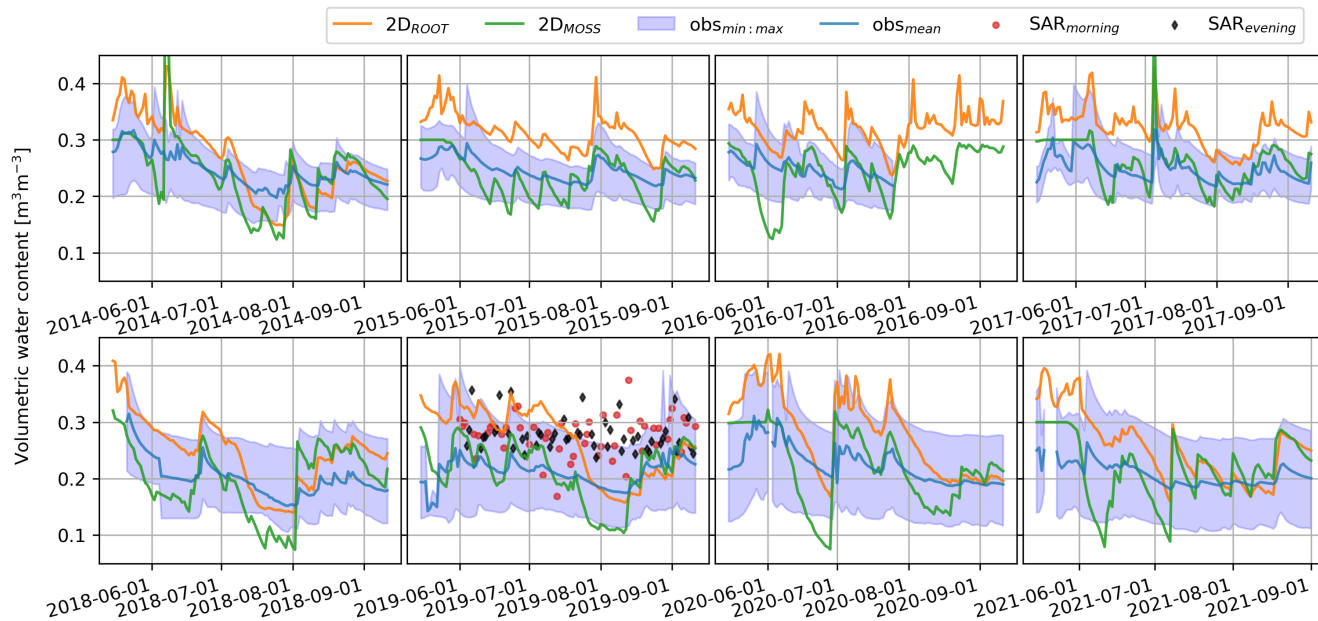


Figure 4. Temporal dynamics of soil moisture at Kenttäröva spruce forest simulated by SpaFHy-2D (rootzone and organic moss-humus layers), measured *in-situ* and estimated from SAR for 2014–2021 during May–Sept period. Simulations and SAR-based estimates correspond to the mean of the nearby grid cells ($64 \times 64 \text{ m}^2$ grid northwest of Kenttäröva). The SAR-based surface soil moisture estimates are only available in 2019.

310 events are better captured by the 2D approach, whereas the baseflow is better predicted by TOP (Fig. S2). The simulations of SWE also align relatively well with the observations at Kenttäröva and Lompolojänkki (Fig. S3). Although catchment-scale ET observations are not available, the good performance in reproducing Q/P -ratio (Fig. 3C) means annual ET is also well described. This is in accordance with the relatively good correspondence between simulated and EC-measured daily ET from Lompolojänkki mire and Kenttäröva spruce forest flux sites (Fig. S4). SpaFHy has also shown earlier to well reproduce the
 315 EC-based ET across the range of boreal and subarctic forests and peatlands (Launiainen et al., 2019).

3.2 Comparison of temporal soil moisture with *in-situ* observations

Intra-seasonal continuous *in-situ* data allow analysis of temporal soil moisture dynamics, and evaluation of models and SAR data (Fig. 4). Soil moisture peaks during snowmelt, and the date of complete snow melt-out corresponds to date when the modeled organic moss-humus layer moisture content begins to drop due to evaporative drying (Fig. 4). Later in the summer,
 320 the soil moisture dynamics are driven by intermittent precipitation events and more continuous drying by ET and drainage, with the general drying trend being dominant (Figs. 4 and 5).

At Kenttäröva hilltop area (Fig. 1A), which contributes to groundwater recharge, the SpaFHy-1D and TOP predictions were nearly identical to SpaFHy-2D. The model well captures the seasonal trend but tends to overestimate both rootzone soil

moisture content and its temporal variability compared to the mean of point observations (Fig. 4, MBE: $0.05 \text{ m}^3\text{m}^{-3}$). This mismatch could be corrected by calibrating soil field capacity and wilting point. However, as the simulations mostly fall within the observed range (MBE: $-0.01 \text{ m}^3\text{m}^{-3}$ when compared to observed maximum) and the comparison in Fig. 4 represents a single location, such calibration was not considered meaningful for the aims of this study.

The SpaFHy-2D also reasonably well predicts the rootzone soil moisture differences between locations, especially in terms of ranking the locations between wet, intermediate and dry (Fig. 5). Minor discrepancies between SpaFHy-2D predicted rootzone and *in-situ* measured shallow soil moisture content are likely due to uncertainties in soil hydraulic parameters (e.g. too large field capacity in Fig. 5A). The moisture content of the organic moss-humus layer is more dynamic than rootzone moisture, as evaporative losses exceed throughfall input leading to drying of the organic moss-humus layer from mid-July to end of August (Fig. 5). SpaFHy-2D does not include capillary rise to the organic moss-humus layer, and therefore simultaneous high evaporation and high water table can create large differences between the moisture contents of the two layers (Fig. 5D,E,G). The largest differences between data and rootzone simulations are found in mixed forested-peatland grid-cells (Fig 5F,G) mostly due to overestimation of the water table level in early summer. Considering that no model calibration was conducted, the comparison of SpaFHy-2D simulated and *in-situ* observed groundwater levels show rather good model performance, and particularly the shallow water tables are well captured (see Fig. S5 and Table S4). As we aim to assess the influence of lateral flow on shallow soil moisture dynamics rather than fully replicate the observations, the performance of the 2D model is considered sufficient.

SAR-based shallow soil moisture mostly fall within the observed range, and the SAR morning flyover captures main temporal dynamics of the observations, particularly drying in June and wetting in late August (Figs. 4 and 5). However, the SAR-based estimates consistently fall short of the highest observed and simulated values, leading to an underestimation of soil moisture content (Fig. 5). There is also noticeable noise in SAR-based soil moisture, and the level and temporal patterns of SAR morning and evening flyovers differ from each other. The comparison at different locations (Fig. 5: two forest, three peatland, and three mixed forested-peatlands grid-cells) shows a systematic shift (up to $0.2 \text{ m}^3\text{m}^{-3}$) between SAR morning and evening flyover.

3.3 Effect of groundwater flow conceptualizations on soil moisture

The *in-situ* soil moisture data is further used to compare the model conceptualizations and to assess the impact of groundwater flow on shallow soil moisture across the catchment (Fig. 6). The comparison shows that the observed soil moisture contents below ca. $0.55 \text{ m}^3\text{m}^{-3}$ are rather well captured by all model conceptualizations (Fig. 6A,B,C), especially considering the uncertainties in soil hydraulic parameters based on geospatial data (Fig. 2: soil type). Most of the forest grid-cells (i.e. grid-cells with high canopy fraction) belong to this category. The results indicate model performance improves when the lateral flows are accounted for, and only the 2D approach with explicit lateral groundwater flow can satisfactorily reproduce the wetter conditions above $0.55 \text{ m}^3\text{m}^{-3}$, commonly found on open peatland grid-cells, and occasionally on forest grid-cells (Fig. 6). Conceptually, the SpaFHy-TOP should also be able to mimic groundwater dynamics via TWI. However, it was able to capture only one of the observed wet grid-cells, and the overall goodness-of-fit is close to the SpaFHy-1D version. All

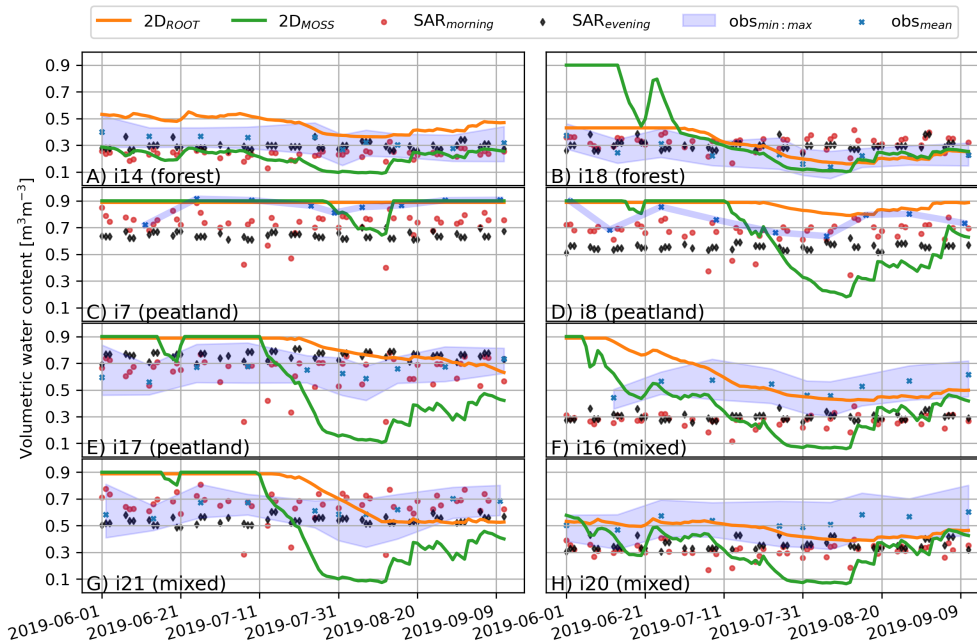


Figure 5. Temporal dynamics of SpaFHy-2D simulated, SAR-estimated and *in-situ* measured range of soil moisture ($obs_{min:max}$) at two forest, three peatland and three mixed forested peatland locations during June–Sept period in 2019.

evaluation metrics are considerably better for the 2D model, but this model variant tends to overestimate soil moisture on peatland grid-cells, consistent with Fig 5F,G.

360 The same comparison, but with colors classifying the points as either mineral soil or peat soil (based on Fig. 2: soil type) in Fig. S6C indicates that many of the grid-cells where model overestimates soil moisture are either faultily parameterized as peat soil, or the model may exaggerate the impact of lateral flow at those locations.

Qualitative spatial evaluation of the model versions in Fig. 7 reveals that the large-scale spatial heterogeneity of shallow soil moisture is most strongly driven by the soil type (see Fig. 2) via the soil hydraulic properties. Particularly the differences in
 365 the 1D simulation arise almost solely from differences in soil types (coarse and medium texture mineral soil and peat), while the role of vegetation heterogeneity appears minimal (Fig. 10). The histograms of 1D simulations show that daily moisture values are distributed around field capacities of mineral and peat soils (Fig. 7), consistent in Fig. S7A where all daily simulated distributions are shown. All model conceptualizations match the drier observations in the upland forest areas rather well, consistent with Fig. 6. However, as the 1D approach neglects groundwater storage and flow, the soil moisture estimates do
 370 not reach the observed high values as drainage rapidly removes water excessive to field capacity. Hence, the 1D simulation is biased low at wet locations (Figs. 6 and 7). Slightly more spatial variability can be seen in the TOP simulation, yet the cells where return flow from groundwater storage is activated remain rare (except close the stream network) even in wet conditions (2021-06-17, Fig. 7B) and almost non-existent in drier autumn conditions (2021-09-01, Fig. 7E).

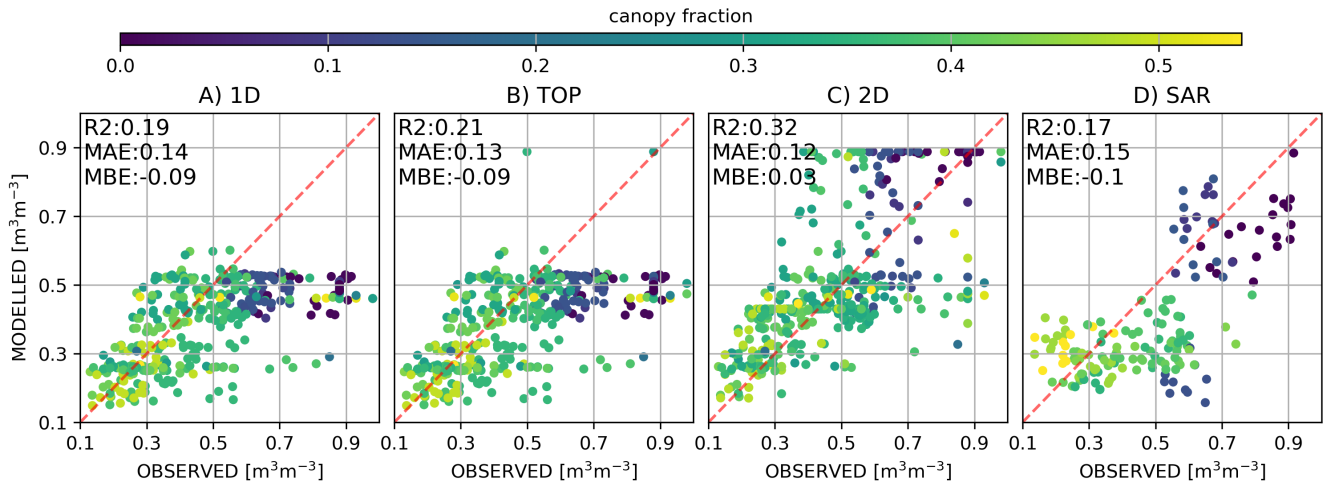


Figure 6. Comparison of simulated rootzone soil moisture content and SAR-based surface soil moisture estimates against spatiotemporal manual *in-situ* soil moisture observations. The color of the points correspond to grid-cell canopy fraction, ranging from open peatlands to forest grid-cells.

The SpaFHy-2D simulates larger saturated areas and match most of the point observations well in Fig 7. Nevertheless, there are still inaccuracies, as saturated conditions adjacent to ditches are not well simulated and the observed variability in forests is not fully captured. The spatial variability of soil moisture in the 2D simulation depends strongly on the water table dynamics. Compared to other model variants, this creates stronger soil moisture variability within the catchment and yields better agreement with the observations. The histograms of Fig. 7C,F and Fig. S7C also show higher frequency for grid-cells to be wet.

380 3.4 Comparison of spatial soil moisture

Previous section suggests that it is necessary to include the lateral groundwater flow to model the spatial patterns of soil moisture at LJO catchment. However, comparison to point measurements can only capture a fraction of the simulated time steps and grid-cells, and comparison with the spatially explicit SAR-based soil moisture is useful. In contrast to the model, SAR-based soil moisture have poorer correspondence with the observations in grid-cells where canopy fraction is high, but provide better match on open and wetter grid-cells (i.e. peatlands, Figs. 6D and S6D). However, it is worth noting that the observations in Figs. 6D and S6D include all measurements in the rootzone (0–30 cm), surpassing the assumed penetration depth of the SAR signal (1–5 cm).

A spatial comparison between SpaFHy-2D and spatially explicit SAR-based soil moisture is shown in Fig. 8. As already noted, the simulated spatial patterns mostly follow soil parameterizations, as well as water table dynamics affected by the lateral flow. The vegetation heterogeneity and consequent differences in rainfall interception and evaporation result in additional variability for simulated organic moss-humus layer moisture in dry conditions (Figs. 5 and 10). SAR and the SpaFHy-2D

rootzone simulations agree on their main spatial patterns (i.e. drier forests and wetter peatlands). A spatiotemporal comparison metrics (Table S5) show that SAR generally predicts lower mean soil moisture and variance (mean, variance = 0.34, 0.02 m^3m^{-3}) than SpaFHy-2D (mean, variance = 0.39, 0.04 m^3m^{-3}), but higher mean soil moisture and variance compared to
395 SpaFHy-1D (mean, variance = 0.29, 0.01 m^3m^{-3}). It is also noticeable from Table S5 that the wet quantiles (0.9) of SpaFHy-2D rootzone (0.82 m^3m^{-3}) and SAR (0.65 m^3m^{-3}) both suggest a major influence of lateral groundwater flow on soil moisture, consistent with earlier findings concerning peatlands (Fig. 8) throughout the season (Fig. 5C,D)

It is likely that SpaFHy-2D overestimates organic moss-humus layer moisture content variability, as there is a clear discrepancy between the SpaFHy-2D and the SAR-based estimates. The simulations provide too high moisture content in wet
400 (Fig. 8A) and are biased low in drier conditions (Fig. 8D). Compared to the simulations, SAR data shows significantly more cell-to-cell variability and the histogram appears nearly normally distributed, especially below 0.55 m^3m^{-3} (mainly mineral soils). Histograms of all daily soil moisture values in Fig. S7D confirm that the SAR data tends to be normally distributed between 0.1 and 0.5 m^3m^{-3} . A closer look at the rectangular box shown in Fig. 8 further confirms the good agreement of SpaFHy-2D -simulated and SAR-estimated rootzone moisture both at the dry and wet areas, but also demonstrates the high
405 cell-to-cell variability in SAR-based soil moisture (Fig. 9).

Considering the ability of SAR to relatively well predict peatland soil moisture (Figs. 6D and S6D), the agreement of SpaFHy-2D and SAR provide support for our earlier findings that soil moisture predictions improve when the lateral groundwater flow is included (SpaFHy-2D). The agreement of SpaFHy-2D and SAR is further supported by a quantitative comparison in Fig. S8, where two clusters of soil moisture emerge in peatlands. The cluster of wet points correspond to the grid-cells with
410 groundwater flow influence, while the other cluster is not impacted by the lateral flow. The consistency between the SAR and SpaFHy-2D is not as clear on mineral soil grid-cells (Fig. S8), likely due to uncertainties in the model's soil hydraulic parameters as well as limitations in SAR soil moisture detection in forests (Fig. 6).

3.5 Drivers of spatiotemporal soil moisture variability

To better separate the role of lateral groundwater flow from that of vegetation heterogeneity under different temporal soil
415 moisture regimes, Fig. 10 shows the grid-cell to grid-cell differences ($\Delta\theta$) between SpaFHy-2D and 1D simulations as well as between 1D and 1D_{homog.canopy} runs. As expected, the difference between SpaFHy-2D and 1D simulations is highest in wet conditions ($q = 0.9$, Fig. 10C). In this case the lateral groundwater flow has a large impact on soil moisture (mean $\Delta\theta$ between 2D and 1D ca. 0.1 m^3m^{-3}) in major part of the catchment, including also parts of the forested areas. The difference between the models is smallest at periods with intermediate soil moisture ($q = 0.5$, mean difference ca. 0.05 m^3m^{-3} , Fig. 10B), during
420 which the lateral flow has an effect almost only in peatland grid-cells. Interestingly, the difference between the 2D and 1D predicted soil moisture becomes significant also in dry conditions (mean difference ca. 0.07 m^3m^{-3} , Fig. 10A), indicating a long-lasting effect of lateral groundwater flow from the upland to the lowland grid-cells. The role of vegetation heterogeneity on soil moisture patterns is negligible at intermediate and wet conditions (Fig. 10E,F), and only minor differences are found in very dry conditions (Fig. 10D). The vegetation heterogeneity plays a larger role in the moisture content of the organic
425 moss-humus layer, but the impact of lateral flow still remains stronger (Fig. S9).

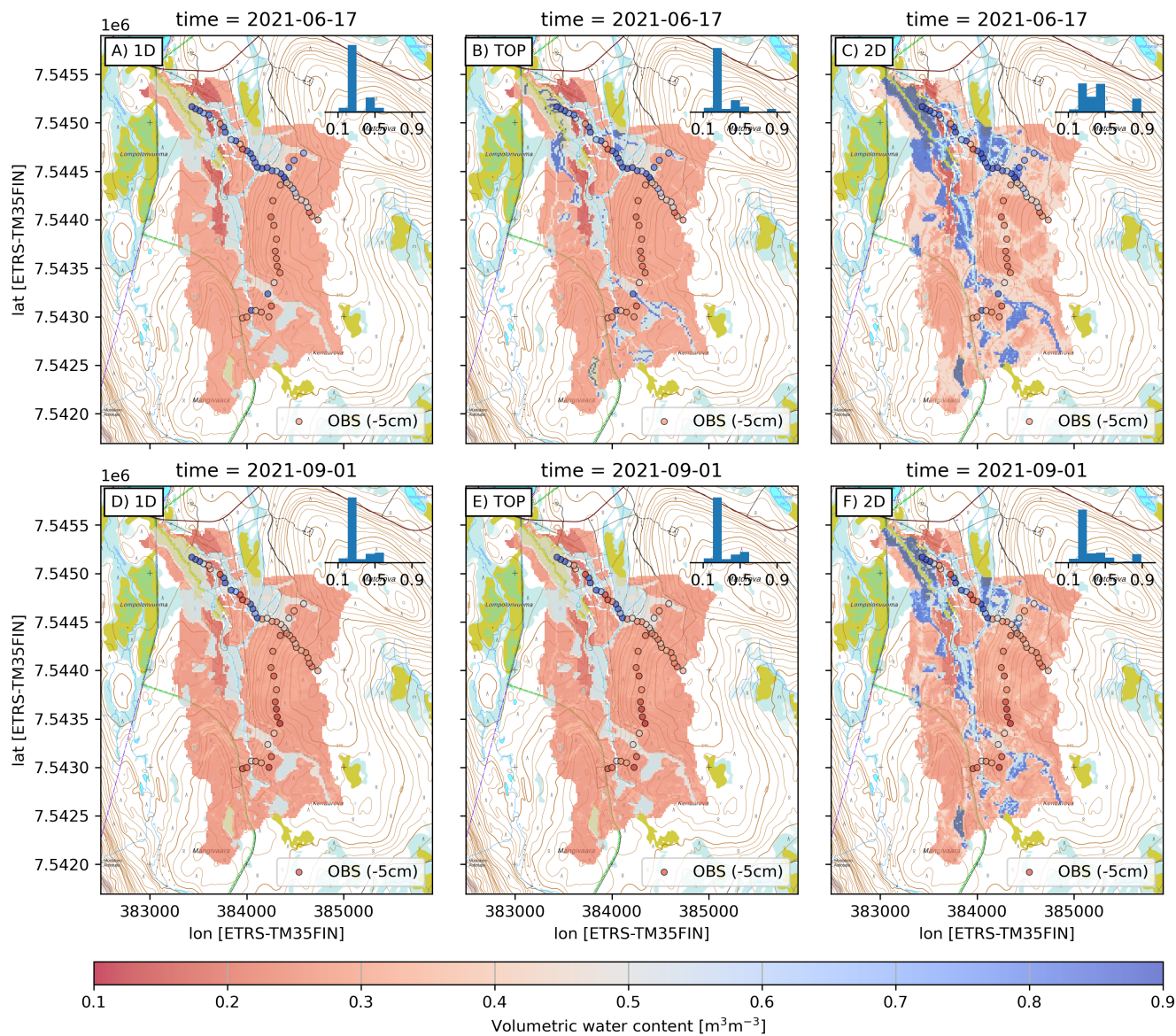


Figure 7. Spatial patterns of modeled rootzone volumetric water content by the three model conceptualizations on 2021-06-17 (upper row, more moist) and 2021-08-01 (lower row, drier conditions). The bar plot shows binned distributions of simulated grid-cell soil moisture across the whole catchment, and *in-situ* measurements at 5 cm depth are shown as circles. The rasters overlay a topographic map (NLSF, 2020).

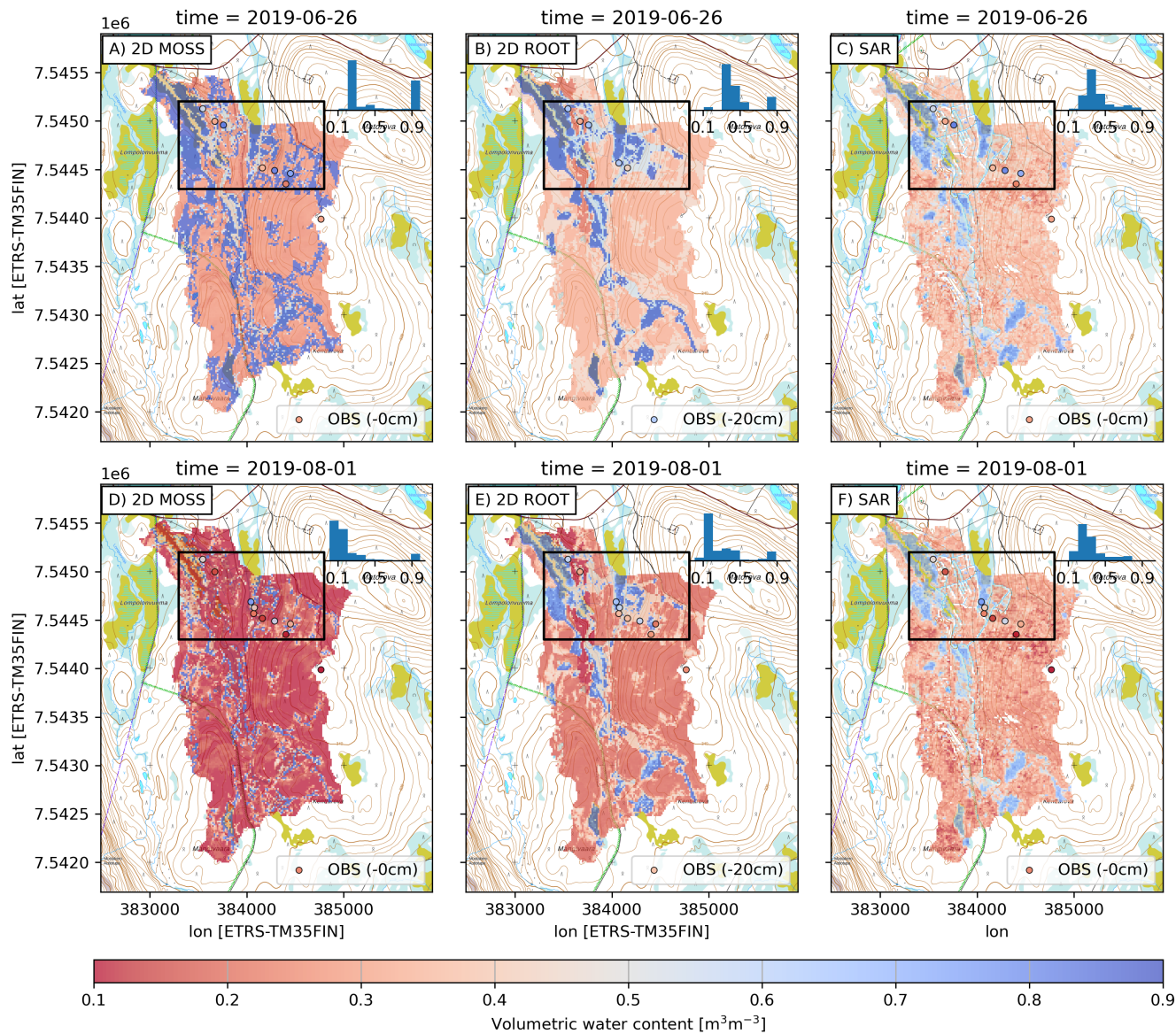


Figure 8. Spatial patterns of SpaFH_y-2D modeled rootzone and organic moss-humus moisture, and SAR-based estimates on wet (2019-06-26, upper row) and dry day (2019-08-01, lower row). *In-situ* measurements at 0 cm and 20 cm depths are shown as circles, and the bar plot shows binned distributions of simulated and SAR-estimated soil moisture across the whole catchment. The rectangular box shows an area that is presented in Fig. 9. The rasters overlay a topographic map (NLSF, 2020).

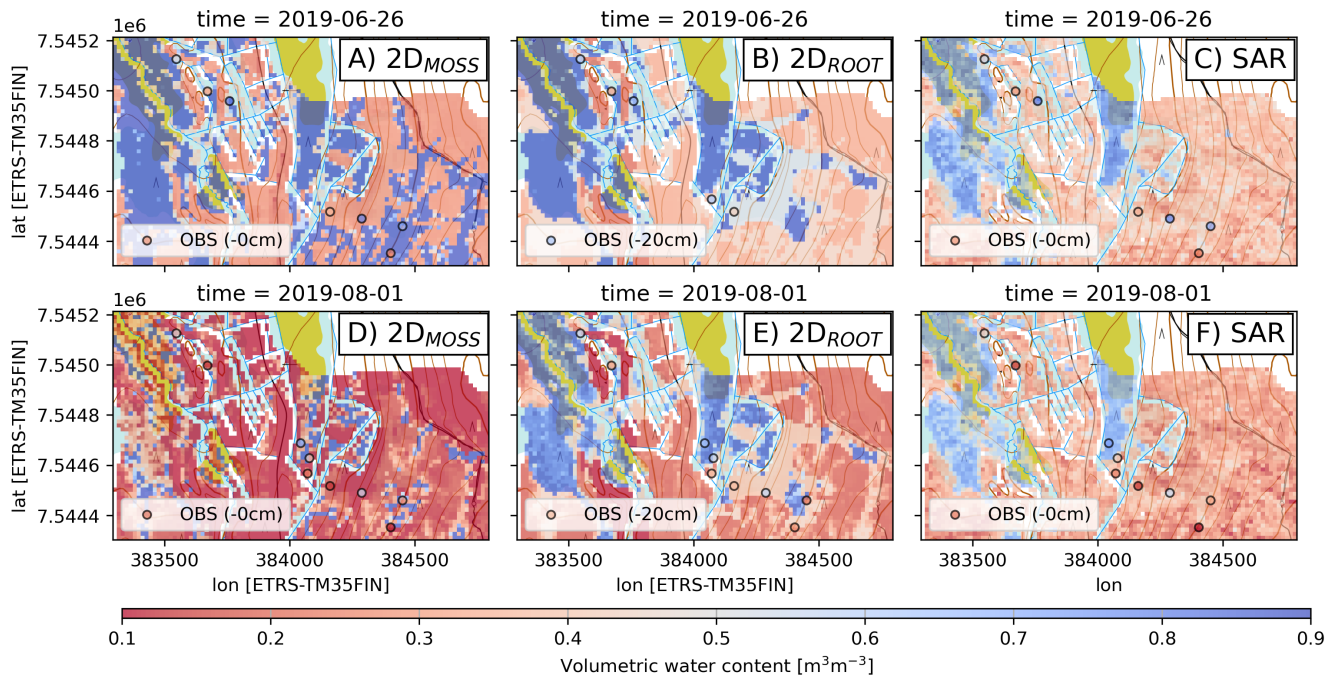


Figure 9. A zoomed in distribution of 2D modeled rootzone and organic moss-humus moisture and SAR-based estimates on wet (2019-06-26, upper row) and dry day (2019-08-01, lower row). *In-situ* measurements at 0 cm and 20 cm depths are shown as circles. The rasters overlay a topographic map (NLSF, 2020).

4 Discussion

4.1 Insights on the role of lateral groundwater flow for shallow soil moisture

Our multi-scale data and high-resolution process-based simulations in the subarctic LJO catchment showed that regardless of the catchment hydrologic state (from dry summer to very moist conditions after snowmelt), lateral groundwater flow plays a major role in shaping the spatial variability of soil moisture (Fig. 10). The results indicate that spatially resolved models, which include groundwater flow are necessary to predict soil moisture variability at high-latitude catchments. Nevertheless, lateral groundwater flow is commonly neglected in current hydrological and land surface models that operate at a coarse resolution (Best et al., 2011; Lawrence et al., 2012; Niu et al., 2011; Noilhan and Mahfouf, 1996). Increasing the spatial resolution of hydrological and biogeochemical land-surface models is the current trend; for instance Wood et al. (2011) set the ambition for future hyper-resolution LSMs to 1 km for global-scale and 100 m for regional-scale simulations. When the models are adapted to finer grids, it becomes increasingly important to implement lateral groundwater dynamics (Ji et al., 2017; Kim and Mohanty, 2016; Decker et al., 2013). Our relatively simple 2D shallow groundwater Darcy flow model, incorporating only 7 additional parameters (water retention parameters, depth-to-bedrock, and stream water level) determined using openly

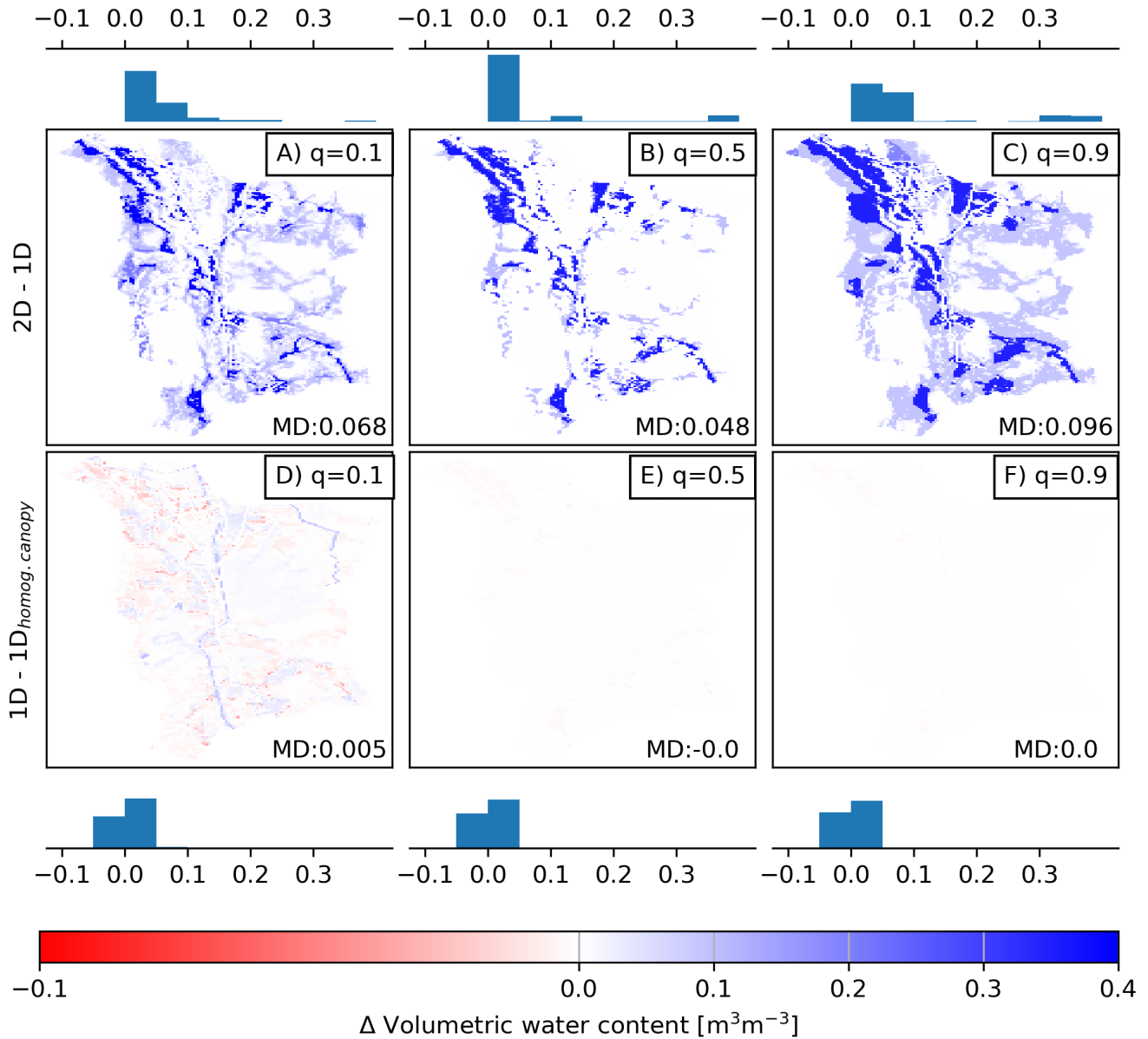


Figure 10. The impact of lateral groundwater flow (upper row) on rootzone soil moisture expressed as simulated $\Delta\theta = 2D - 1D$, and the impact of vegetation heterogeneity (bottom row) expressed as simulated $\Delta\theta = 1D - 1D_{homog.canopy}$ in different catchment soil moisture states. The panels correspond to 0.1, 0.5, and 0.9 quantiles of grid-cell soil moisture, and the bars show distribution of binned differences. Mean difference (MD) is shown in each panel. Note that blank panel refers to $\Delta\theta = 0.0 \text{ m}^3\text{m}^{-3}$.

available digital elevation model, soil type and stream network rasters, performed comparably to the state-of-the-art integrated
440 surface-groundwater model HydroGeoSphere (Brunner and Simmons, 2012) in predicting observed groundwater levels at the
LJO catchment (compare Fig. S6 and Table S4 in our Supplement, and Fig. 6 and Table S6 in Autio et al. (2023)). Also, the
groundwater influenced areas in the catchment are in broad agreement with the simulations by Autio et al. (2023).

Regardless of the known sensitivity of ecohydrological fluxes (i.e. interception, evaporation, transpiration) to changes in
445 LAI and plant type (Launiainen et al., 2019; Kozii et al., 2020; Launiainen et al., 2016), the impact of lateral groundwater
flow outweighed the impact of vegetation heterogeneity on soil moisture dynamics throughout the year. However, the growing
season in Pallas is short and vegetation rather sparse and not very heterogeneous within the site classes (Fig. 2). In addition,
the impact of vegetation heterogeneity on soil moisture is attenuated due to the compensating processes; soil evaporation
decreases while transpiration and interception evaporation increase with increasing LAI, resulting in less drastic changes in
450 total ET (Leppä et al., 2020; Launiainen et al., 2019). Consistent with Kollet and Maxwell (2008), the impact of groundwater
flow on shallow soil moisture persisted also in dry conditions, suggesting high resilience of lowlands to droughts due to
long-lasting lateral flow from the upland part of the catchment. The simulations showed that for large parts of the catchment
rootzone moisture content was controlled by lateral groundwater flow, and the strength of this effect depends on the state of
the groundwater storage. Ji et al. (2017) showed that the role of lateral water flow becomes crucial in high-resolution land
455 surface simulations in a region dominated by a humid climate and coniferous forests in the western USA. At a resolution of
100 meters, they showed that subsurface lateral flow transports moisture from high elevation areas to valley bottoms, impacting
local grid-cell and catchment average ET especially in dry conditions. Kollet and Maxwell (2008) coupled a groundwater and a
land surface model, and demonstrated that when the water table depth was above 5 meters, there was strong coupling between
groundwater dynamics and land surface processes at the subhumid grassland-dominated watershed in the USA. Our results at
460 LJO catchment are in line with these studies regarding the importance of groundwater flow on shallow soil moisture.

The impact of lateral flow was found especially important for peatlands, both due to the high porosity of peat (Menberu
et al., 2021) and location in the valley bottom (Figs. 2, 7 and 8). Mineral forest top soils can also be (temporarily) impacted
by lateral flow, especially soon after strong precipitation events and snowmelt. However, the difference between 1D and 2D
models remained smaller due to the small difference in mineral soil field capacity and porosity (Fig. 10).

465 **4.2 SAR-based soil moisture: Potential and limitations**

The Sentinel-1 SAR-based soil moisture estimates were useful to supplement the point-scale *in-situ* measurements and confirm
the plausibility of the spatial soil moisture predicted by the SpaFHy-2D. To this date, model developments and evaluations of
soil moisture predictions in boreal and subarctic forests and peatlands have been typically limited to point-scale studies, which
fails to encompass the full spatiotemporal extent that distributed hydrological models are simulating (Launiainen et al., 2015;
470 Ala-aho et al., 2017b; Tyystjärvi et al., 2022). We found SAR-estimates useful for spatial model-data comparison, and envision
SAR to have further potential, for instance, as a proxy for water table depth assimilation or improved estimates of topographic
wetness indices (TWI, depth-to-water) in peatlands (Bechtold et al., 2020; Zhang et al., 2018).

The comparison between SAR-based estimates and modeled soil moisture was not straightforward and revealed limitations in using the SAR-based data, for instance as ground-truth calibration data for hydrological models. A direct comparison is 475 challenging due to the disparate penetration depth of SAR in soil (1–5 cm: Nolan and Fatland (2003)), contrasting with the model layering (rootzone layer of 0–30 cm). Indeed, the correspondence of SAR-based estimates against *in-situ* measurements in the rootzone (0–30 cm, Fig. 6) was poorer than the original validation of SAR-estimates against *in-situ* measurements at the surface soil (0 cm, Fig. 11 in Manninen et al. (2021)). This vertical mismatch is a common challenge (Shellito et al., 2020), and hence, enhancing the comparability of *in-situ* measurement as well as hydrological models with SAR-estimates would 480 contribute to more effectively harnessing the SAR-based data. Another notable difference is that hydrological models such as SpaFHy neglect heterogeneity within the grid-cells, while SAR-estimates can integrate multiple backscattering signals for a given grid-cell (Manninen et al., 2021). In turn, hydrological models can integrate temporal information, whereas SAR-based estimates are instantaneous.

We also emphasize the need for potential algorithm improvements in computing soil moisture from SAR signals. Given 485 the homogeneity of the vegetation and soil texture, some of the spatial variability in the SAR-based data appeared more as noise than realistic soil moisture patterns. The different SAR incidence and view angles with respect to the topography, to a large extent, cause the systematic difference of the soil moisture estimates from the morning and evening flyover times (Figs. 4 and 5). Indeed, topography-induced shading posed a significant challenge for the development of the evening soil moisture algorithm for SAR-based estimates (Manninen et al., 2021). Consequently, Manninen et al. (2021) reported higher RMSEs for 490 the evening ($0.088 \text{ m}^3\text{m}^{-3}$) than for the morning flyover ($0.065 \text{ m}^3\text{m}^{-3}$) while the maximum errors were relatively similar ($0.341 \text{ m}^3\text{m}^{-3}$ for morning and $0.339 \text{ m}^3\text{m}^{-3}$ for evening flyover). Further discussion on the differences between these SAR flyovers can be found in Manninen et al. (2021).

Although the SAR-based soil moisture fell mostly within the observed range, the temporal variability and seasonal patterns, especially from the evening flyovers, were small and followed neither the simulated nor *in-situ* observed shallow soil moisture 495 (Fig. 5). The morning flyover occasionally captured some temporal dynamics observed and simulated (see e.g. Fig. 5D). The SAR-based estimates do not reach the highest observed or simulated values, resulting in underestimation of the soil moisture content, likely because they integrate information from multiple signals within a given grid-cell that have been averaged to correspond to the model grid. The presence of different vegetation characteristics and soil textures further complicates the interpretation of the backscattering signals, leading to uncertainties and noise in soil moisture estimates.

500 Overall, the capability of any remote sensing based soil moisture estimate to represent various meteorological and landscape conditions can only be as good as the training data. As acquiring high quality and representative *in-situ* soil moisture data is challenging and costly, we encourage deeper collaboration between hydrological measurements, modeling and remote sensing communities.

4.3 Model limitations and outlook

505 The modularity of SpaFHy (Launiainen et al., 2019) was ideal for comparing the impact of different conceptualizations of the lateral groundwater flow. Nevertheless, there are potentially relevant hydrological processes that are not yet represented. For

instance, overland flow and soil freezing and thawing are currently omitted, and this may influence soil moisture dynamics, particularly during and after snowmelt and in the autumn (Ala-Aho et al., 2021). Lateral overland flow has been found to distribute water from saturated grid-cells to unsaturated areas (e.g. in subarctic tundra and boreal forests; Tang et al., 2014).
510 We suspect that it may be especially important after snowmelt and heavy precipitation events on the low-lying flat peatlands of the catchment. The snowpack representation of SpaFHy successfully captured the snowmelt timing (Figs. S2 and S3), but relies on a simple degree-day approach, potentially limiting its ability to fully capture snowmelt dynamics. Moreover, the radiation conditions on the forest floor within a specific grid-cell may be influenced by the forest canopy in the surroundings. Thus, employing 3D radiation transfer schemes that consider the shading from grid-cell neighbours (Webster et al., 2023), or the
515 demography of individual trees within a grid-cell could be beneficial (Mazzotti et al., 2021).

Although the explicit 2D lateral groundwater flow module added process realism and improved shallow soil moisture predictions, the simulations were still far from perfect, due to uncertainties in classifying soil types and because soil moisture data was not used to calibrate the model's hydraulic parameters. The improvement also comes with a computational cost: in terms of running time, SpaFHy-2D is approximately sixty times slower than TOP and 1D versions. For instance, a one-year
520 simulation with 1D and TOP was completed in 5.4 seconds, while 2D took 321.6 seconds. This can become a burden when applying the 2D model to large areas, or when parameter calibration or ensemble simulations are done.

Uncertainties in model simulations and model evaluation accumulate from multiple sources: input data, model parameters, model structure and errors in *in-situ* measurements (Moges et al., 2021). The meteorological forcing timeseries was constructed from observations at the upland forest site, and radiation data gaps were filled with ERA5 data (Hersbach et al., 2020). It is
525 known that there are intrinsic uncertainties in meteorological observations (Stuefer et al., 2020). Although data gaps were limited, those filled by ERA5 data further add uncertainties in the model-data comparison (Raleigh et al., 2015). In addition, we used spatially uniform meteorological forcing (excluding radiation where topographic shading was accounted for) measured at the forest site that may have been slightly different to those experienced on the lowland peatlands (Aurela et al., 2015).

The model was initiated and parameterized based on the best available open geospatial data on the landscape characteristics.
530 As Härkönen et al. (2015) found a good agreement between the mNFI-based and ground-based LAI estimates, and soil moisture patterns were not majorly altered by vegetation characteristics (Fig. 10), we assume that vegetation parameters did not create marked biases in the soil moisture predictions. However, estimating soil hydraulic properties from available geospatial datasets is challenging (Launiainen et al., 2022) and can yield systematic uncertainties and biased local soil moisture. Modeling lateral groundwater flow by the proposed 2D Darcy scheme also requires distributed data on depth-to-bedrock. As such information
535 was not readily available, these parameters were assigned as estimates. Even with these limitations, the modeled groundwater level dynamics were relatively close to the observed levels (Fig. S5 and Table S4)

5 Conclusions

We explored the controls of high-resolution soil moisture dynamics, particularly the role of lateral groundwater flow, in the subarctic Lompolojängänoja catchment in northwestern Finland. We combined soil moisture data from multiple sources, including

540 *in-situ* measurements and Sentinel-1 SAR-based estimates, and interpreted soil moisture variability with high-resolution ($16 \times 16 \text{ m}^2$) process-based hydrological modeling. To accomplish this, we extended the Spatial Forest Hydrology (SpaFHy) model with an explicit lateral groundwater (2D Darcy flow) submodel, and compared it to existing approaches where lateral groundwater flow was either neglected (free drainage) or based on a simple TOPMODEL conceptualization. The results showed the major impact of lateral groundwater flow in shaping soil moisture dynamics, particularly post snowmelt and after heavy rain-
545 fall. The inclusion of the lateral groundwater flow model notably improved soil moisture simulations in forested peatlands and open peatlands. The soil moisture simulations were affected by uncertainties in hydraulic parameters, which were assigned based on geospatial data on soil types. SAR-based soil moisture estimates were valuable in confirming modeled spatial patterns. Discrepancies in spatial resolutions, SAR penetration depth, and model layering, however, hampered direct comparison. Moreover, the noise in SAR-based data, particularly under forested areas, complicates its use as ground-truth evaluation data
550 for hydrological models. Our study provides novel insights and tools for predicting soil moisture dynamics at high-resolution, necessary for ecohydrological, biogeochemical, and climate change adaptation studies, as well as for land-use management and planning in high-latitude environments.

Code and data availability. SpaFHy model version developed and used in this study is available at Nousu et al. (2024a). The code repository also includes meteorological forcing files and geospatial input rasters.

555 *In-situ* hydrological measurement data, including soil moisture, evapotranspiration, groundwater levels, and specific discharge, are available at Nousu et al. (2024b).

Author contributions. JPN, SL, PA and HM designed the research. JPN led the study and performed the model experiments and data analysis, with scientific contributions of KL, SL, GM, HM, TM and PA. *In-situ* manual measurements were conducted by JPN and MK. JPN was responsible for writing the article, with contributions from all authors. MA and AL provided the energy flux data, and TM provided the SAR
560 data. SL, HM, PA and AL were responsible for the funding acquisition.

Competing interests. The contact author has declared that none of the authors has any competing interests.

Acknowledgements. This work was funded by the Research Council of Finland (RCF) (ArcI Profi 4). Giulia Mazzotti was funded by the Swiss National Science Foundation (grant no. P500PN_202741). Samuli Launiainen and Jari-Pekka Nousu acknowledge the GreenFeed-Back project from the EU Horizon Europe Framework Programme for Research and Innovation (grant no. 101056921). Samuli Launiainen
565 acknowledges the support of RCF (no. 356138 & 348102). Pertti Ala-aho was funded by the RCF Research Fellow grant (no. 347348). We acknowledge the Ministry of Transport and Communications through the Integrated Carbon Observing System (ICOS), ICOS Finland and

RCF (grant no. 308511). The authors would like to thank Emmihenna Jääskeläinen and Anna Autio for valuable discussions during this work. We also acknowledge the use of ChatGPT 3.5 (Open AI, <https://chat.openai.com>) to proofread parts of the paper.

References

- 570 Ala-aho, P., Soulsby, C., Wang, H., and Tetzlaff, D.: Integrated surface-subsurface model to investigate the role of groundwater in headwater catchment runoff generation: A minimalist approach to parameterisation, *Journal of Hydrology*, 547, 664–677, <https://doi.org/10.1016/j.jhydrol.2017.02.023>, 2017a.
- Ala-aho, P., Tetzlaff, D., McNamara, J., Laudon, H., and Soulsby, C.: Using isotopes to constrain water flux and age estimates in snow-influenced catchments using the STARR (Spatially distributed Tracer-Aided Rainfall-Runoff) model, *Hydrology and Earth System Sciences Discussions*, pp. 1–38, <https://doi.org/10.5194/hess-2017-106>, 2017b.
- 575 Ala-Aho, P., Autio, A., Bhattacharjee, J., Isokangas, E., Kujala, K., Marttila, H., Menberu, M., Meriö, L. J., Postila, H., Rauhala, A., Ronkanen, A. K., Rossi, P. M., Saari, M., Haghighi, A. T., and Klove, B.: What conditions favor the influence of seasonally frozen ground on hydrological partitioning? A systematic review, *Environmental Research Letters*, 16, <https://doi.org/10.1088/1748-9326/abe82c>, 2021.
- Ameray, A., Cavard, X., and Bergeron, Y.: Climate change may increase Quebec boreal forest productivity in high latitudes by shifting its current composition, *Frontiers in Forests and Global Change*, 6, 1–19, <https://doi.org/10.3389/ffgc.2023.1020305>, 2023.
- 580 Aurela, M., Lohila, A., Tuovinen, J. P., Hatakka, J., Penttilä, T., and Laurila, T.: Carbon dioxide and energy flux measurements in four northern-boreal ecosystems at Pallas, *Boreal Environment Research*, 20, 455–473, 2015.
- Autio, A., Ala-Aho, P., Rossi, P. M., Ronkanen, A.-K., Aurela, M., Lohila, A., Korpelainen, P., Kumpula, T., Klöve, B., and Marttila, H.: Groundwater exfiltration pattern determination in the sub-arctic catchment using thermal imaging, stable water isotopes and fully-integrated groundwater-surface water modelling, *Journal of Hydrology*, 626, 130–134, <https://doi.org/10.1016/j.jhydrol.2023.130342>, 2023.
- 585 Bauer-Marschallinger, B., Freeman, V., Cao, S., Paulik, C., Schaufler, S., Stachl, T., Modanesi, S., Massari, C., Ciabatta, L., Brocca, L., and Wagner, W.: Toward Global Soil Moisture Monitoring With Sentinel-1: Harnessing Assets and Overcoming Obstacles, *IEEE Transactions on Geoscience and Remote Sensing*, 57, 520–539, <https://doi.org/10.1109/TGRS.2018.2858004>, 2019.
- 590 Beale, J., Waine, T., Evans, J., and Corstanje, R.: A Method to Assess the Performance of SAR-Derived Surface Soil Moisture Products, *IEEE Journal of Selected Topics in Applied Earth Observations and Remote Sensing*, 14, 4504–4516, <https://doi.org/10.1109/JSTARS.2021.3071380>, 2021.
- Bechtold, M., De Lannoy, G. J., Reichle, R. H., Roose, D., Balliston, N., Burdun, I., Devito, K., Kurbatova, J., Strack, M., and Zarov, E. A.: Improved groundwater table and L-band brightness temperature estimates for Northern Hemisphere peatlands using new model physics and SMOS observations in a global data assimilation framework, *Remote Sensing of Environment*, 246, 111–118, <https://doi.org/10.1016/j.rse.2020.111805>, 2020.
- 595 Bergström, S.: The HBV model - its structure and applications, Swedish Meteorological and Hydrological Institute, Norrköping, 4, 1–33, 1992.
- Best, M. J., Pryor, M., Clark, D. B., Rooney, G. G., Essery, R. L. H., Ménard, C. B., Edwards, J. M., Hendry, M. A., Porson, A., Gedney, N., Mercado, L. M., Sitch, S., Blyth, E., Boucher, O., Cox, P. M., Grimmond, C. S. B., and Harding, R. J.: The Joint UK Land Environment Simulator (JULES), model description – Part 1: Energy and water fluxes, *Geoscientific Model Development*, 4, 677–699, <https://doi.org/10.5194/gmd-4-677-2011>, 2011.
- 600 Beven, K. J. and Kirkby, M. J.: A physically based, variable contributing area model of basin hydrology, *Hydrological Sciences Bulletin*, 24, 43–69, <https://doi.org/10.1080/02626667909491834>, 1979.
- 605 Bhattarai, N. and Wagle, P.: Recent Advances in Remote Sensing of Evapotranspiration, <https://doi.org/10.3390/rs13214260>, 2021.

- Bonan, G. B.: Carbon and Nitrogen Cycling in North American Boreal Forests . I . Litter Quality and Soil Thermal Effects in Interior Alaska, *Biogeochemistry*, 10, 1–28, 1990.
- Bond-Lamberty, B., Smith, A. P., and Bailey, V.: Temperature and moisture effects on greenhouse gas emissions from deep active-layer boreal soils, *Biogeosciences*, 13, 6669–6681, <https://doi.org/10.5194/bg-13-6669-2016>, 2016.
- 610 Brunner, P. and Simmons, C. T.: HydroGeoSphere: A Fully Integrated, Physically Based Hydrological Model, *Groundwater*, 50, 170–176, <https://doi.org/https://doi.org/10.1111/j.1745-6584.2011.00882.x>, 2012.
- Buermann, W., Parida, B., Jung, M., MacDonald, G. M., Tucker, C. J., and Reichstein, M.: Recent shift in Eurasian boreal forest greening response may be associated with warmer and drier summers, *Geophysical Research Letters*, 41, 1995–2002, <https://doi.org/https://doi.org/10.1002/2014GL059450>, 2014.
- 615 Celik, M. F., Isik, M. S., Yuzugullu, O., Fajraoui, N., and Erten, E.: Soil Moisture Prediction from Remote Sensing Images Coupled with Climate, Soil Texture and Topography via Deep Learning, <https://doi.org/10.3390/rs14215584>, 2022.
- Clark, M. P., Slater, A. G., Rupp, D. E., Woods, R. A., Vrugt, J. A., Gupta, H. V., Wagener, T., and Hay, L. E.: Framework for Understanding Structural Errors (FUSE): A modular framework to diagnose differences between hydrological models, *Water Resources Research*, 44, <https://doi.org/10.1029/2007wr006735>, 2008.
- 620 Clark, M. P., Nijssen, B., Lundquist, J. D., Kavetski, D., Rupp, D. E., Woods, R. A., Freer, J. E., Gutmann, E. D., Wood, A. W., Brekke, L. D., Arnold, J. R., Gochis, D. J., and Rasmussen, R. M.: A unified approach for process-based hydrologic modeling: 1. Modeling concept, *Water Resources Research*, 51, 2498–2514, <https://doi.org/10.1002/2015WR017200.A>, 2015.
- Corradini, C.: Soil moisture in the development of hydrological processes and its determination at different spatial scales, *Journal of Hydrology*, 516, 1–5, <https://doi.org/10.1016/j.jhydrol.2014.02.051>, 2014.
- 625 Crow, W. T. and Yilmaz, M. T.: The auto-tuned land data assimilation system (ATLAS), *Water Resources Research*, 50, 371–385, <https://doi.org/10.1002/2013WR014550>, 2014.
- Daly, E. and Porporato, A.: A review of soil moisture dynamics: From rainfall infiltration to ecosystem response, *Environmental Engineering Science*, 22, 9–24, <https://doi.org/10.1089/ees.2005.22.9>, 2005.
- De Lannoy, G. J. M., Bechtold, M., Albergel, C., Brocca, L., Calvet, J.-C., Carrassi, A., Crow, W. T., de Rosnay, P., Durand, M., Forman, B., Geppert, G., Giroto, M., Hendricks Franssen, H.-J., Jonas, T., Kumar, S., Lievens, H., Lu, Y., Massari, C., Pauwels, V. R. N., Reichle, R. H., and Steele-Dunne, S.: Perspective on satellite-based land data assimilation to estimate water cycle components in an era of advanced data availability and model sophistication, *Frontiers in Water*, 4, <https://doi.org/10.3389/frwa.2022.981745>, 2022.
- Decharme, B., Delire, C., Minvielle, M., Colin, J., Vergnes, J. P., Alias, A., Saint-Martin, D., S  f  rian, R., S  n  si, S., and Voldoire, A.: Recent Changes in the ISBA-CTRIP Land Surface System for Use in the CNRM-CM6 Climate Model and in Global Off-Line Hydrological Applications, *Journal of Advances in Modeling Earth Systems*, 11, 1207–1252, <https://doi.org/10.1029/2018MS001545>, 2019.
- 635 Decker, M., Pitman, A. J., and Evans, J. P.: Groundwater constraints on simulated transpiration variability over Southeastern Australian forests, *Journal of Hydrometeorology*, 14, 543–559, <https://doi.org/10.1175/JHM-D-12-058.1>, 2013.
- Deschamps-Berger, C., Cluzet, B., Dumont, M., Lafaysse, M., Berthier, E., Fanise, P., and Gascoign, S.: Improving the Spatial Distribution of Snow Cover Simulations by Assimilation of Satellite Stereoscopic Imagery, *Water Resources Research*, 58, e2021WR030271, <https://doi.org/https://doi.org/10.1029/2021WR030271>, 2022.
- 640 Dobriyal, P., Qureshi, A., Badola, R., and Hussain, S. A.: A review of the methods available for estimating soil moisture and its implications for water resource management, *Journal of Hydrology*, 458-459, 110–117, <https://doi.org/10.1016/j.jhydrol.2012.06.021>, 2012.

- Elumeeva, T. G., Soudzilovskaia, N. A., Daring, H. J., and Cornelissen, J. H.: The importance of colony structure versus shoot morphology for the water balance of 22 subarctic bryophyte species, *Journal of Vegetation Science*, 22, 152–164, <https://doi.org/10.1111/j.1654-1103.2010.01237.x>, 2011.
- Esri: ESRI Satellite (ArcGIS/World_Imagery), <https://www.arcgis.com/home/item.html?id=10df2279f9684e4a9f6a7f08febac2a9>, 2023.
- Essery, R., Pomeroy, J., Parviainen, J., and Storck, P.: Sublimation of snow from coniferous forests in a climate model, *Journal of Climate*, 16, 1855–1864, [https://doi.org/10.1175/1520-0442\(2003\)016<1855:SOSFCF>2.0.CO;2](https://doi.org/10.1175/1520-0442(2003)016<1855:SOSFCF>2.0.CO;2), 2003.
- FMI: Finnish Meteorological Institute past weather observations, available at: <https://en.ilmatieteenlaitos.fi/download-observations>, 2021.
- GSF: Geological Survey of Finland, bedrock 1:200 000 and superficial deposits 1:20 000 and 1:50 000, available at: <https://hakku.gtk.fi/en>, 2020.
- Gupta, H. V., Kling, H., Yilmaz, K. K., and Martinez, G. F.: Decomposition of the mean squared error and NSE performance criteria: Implications for improving hydrological modelling, *Journal of Hydrology*, 377, 80–91, <https://doi.org/https://doi.org/10.1016/j.jhydrol.2009.08.003>, 2009.
- Härkönen, S., Lehtonen, A., Manninen, T., Tuominen, S., and Peltoniemi, M.: Estimating forest leaf area index using satellite images: comparison of k-NN based Landsat-NFI LAI with MODISRSR based LAI product for Finland, *Boreal Environment Research*, 20, 181–195, 2015.
- Hersbach, H., Bell, B., Berrisford, P., Hirahara, S., Horányi, A., Muñoz-Sabater, J., Nicolas, J., Peubey, C., Radu, R., Schepers, D., Simmons, A., Soci, C., Abdalla, S., Abellan, X., Balsamo, G., Bechtold, P., Biavati, G., Bidlot, J., Bonavita, M., De Chiara, G., Dahlgren, P., Dee, D., Diamantakis, M., Dragani, R., Flemming, J., Forbes, R., Fuentes, M., Geer, A., Haimberger, L., Healy, S., Hogan, R. J., Hólm, E., Janisková, M., Keeley, S., Laloyaux, P., Lopez, P., Lupu, C., Radnoti, G., de Rosnay, P., Rozum, I., Vamborg, F., Villaume, S., and Thépaut, J. N.: The ERA5 global reanalysis, *Quarterly Journal of the Royal Meteorological Society*, 146, 1999–2049, <https://doi.org/10.1002/qj.3803>, 2020.
- Holmberg, M., Futter, M. N., Kotamäki, N., Fronzek, S., Forsius, M., Kiuru, P., Pirttioja, N., Rasmus, K., Starr, M., and Vuorenmaa, J.: Effects of changing climate on the hydrology of a boreal catchment and lake DOC - probabilistic assessment of a dynamic model chain, *Boreal Environment Research*, 19, 66–82, 2014.
- Huttunen, J. T., Nykänen, H., Turunen, J., and Martikainen, P. J.: Methane emissions from natural peatlands in the northern boreal zone in Finland, Fennoscandia, *Atmospheric Environment*, 37, 147–151, [https://doi.org/10.1016/S1352-2310\(02\)00771-9](https://doi.org/10.1016/S1352-2310(02)00771-9), 2003.
- IPCC: Chapter 2: Land–climate interactions, *Climate Change and Land: an IPCC special report on climate change, desertification, land degradation, sustainable land management, food security, and greenhouse gas fluxes in terrestrial ecosystems*, pp. 131–248, 2019.
- Isoaho, A., Ikkala, L., Marttila, H., Hjort, J., Kumpula, T., Korpelainen, P., and Räsänen, A.: Spatial water table level modelling with multi-sensor unmanned aerial vehicle data in boreal aapa mires, *Remote Sensing Applications: Society and Environment*, 32, 101 059, <https://doi.org/https://doi.org/10.1016/j.rsase.2023.101059>, 2023.
- Iwata, Y., Miyamoto, T., Kameyama, K., and Nishiya, M.: Effect of sensor installation on the accurate measurement of soil water content, *European Journal of Soil Science*, 68, 817–828, <https://doi.org/https://doi.org/10.1111/ejss.12493>, 2017.
- J.-P. Vergnes, B. D. and Habets, F.: Introduction of groundwater capillary rises using subgrid spatial variability of topography into, *Journal of Geophysical Research*, pp. 6578–6595, <https://doi.org/10.1002/2014JD021573>. Received, 2014.
- Ji, P., Yuan, X., and Liang, X. Z.: Do Lateral Flows Matter for the Hyperresolution Land Surface Modeling?, *Journal of Geophysical Research: Atmospheres*, 122, 077–12, <https://doi.org/10.1002/2017JD027366>, 2017.

- 680 Jokinen, P., Pirinen, P., Kaukoranta, J.-P., Kangas, A., Alenius, P., Eriksson, P., Johansson, M., and Wilkman, S.: Climatological and oceanographic statistics of Finland 1991–2020, Tech. rep., <http://hdl.handle.net/10138/336063>, 2021.
- Joo, J. and Tian, Y.: Impact of Stream-Groundwater Interactions on Peak Streamflow in the Floods, <https://doi.org/10.3390/hydrology8030141>, 2021.
- Junttila, S., Campos, M., Hölttä, T., Lindfors, L., Issaoui, A. E., Vastaranta, M., Hyypä, H., and Puttonen, E.: Tree Water Status Affects
685 Tree Branch Position, *Forests*, 13, <https://doi.org/10.3390/f13050728>, 2022.
- Kalliokoski, T., Pennanen, T., Nygren, P., Sievänen, R., and Helmisaari, H. S.: Belowground interspecific competition in mixed boreal forests: Fine root and ectomycorrhiza characteristics along stand developmental stage and soil fertility gradients, *Plant and Soil*, 330, 73–89, <https://doi.org/10.1007/s11104-009-0177-9>, 2010.
- Kankare, V., Luoma, V., Saarinen, N., Peuhkurinen, J., Holopainen, M., and Vastaranta, M.: Assessing feasibility of the forest trafficability
690 map for avoiding rutting – A case study, *Silva Fennica*, 53, 1–9, <https://doi.org/10.14214/sf.10197>, 2019.
- Karhu, K., Auffret, M. D., Dungait, J. A., Hopkins, D. W., Prosser, J. I., Singh, B. K., Subke, J. A., Wookey, P. A., Agren, G. I., Sebastià, M. T., Gouriveau, F., Bergkvist, G., Meir, P., Nottingham, A. T., Salinas, N., and Hartley, I. P.: Temperature sensitivity of soil respiration rates enhanced by microbial community response., *Nature*, 513, 81–84, <https://doi.org/10.1038/nature13604>, 2014.
- Kemppinen, J., Niittynen, P., Rissanen, T., Tyystjärvi, V., Aalto, J., and Luoto, M.: Soil Moisture Variations From Boreal Forests to the
695 Tundra, *Water Resources Research*, 59, e2022WR032719, <https://doi.org/https://doi.org/10.1029/2022WR032719>, 2023.
- Kim, J. and Mohanty, B. P.: Influence of lateral subsurface flow and connectivity on soil water storage in land surface modeling, *Journal of Geophysical Research: Atmospheres*, 121, 704–721, <https://doi.org/https://doi.org/10.1002/2015JD024067>, 2016.
- Kløve, B., Ala-Aho, P., Bertrand, G., Gurdak, J. J., Kupfersberger, H., Kvarner, J., Muotka, T., Mykrä, H., Preda, E., Rossi, P., Uvo, C. B., Velasco, E., and Pulido-Velazquez, M.: Climate change impacts on groundwater and dependent ecosystems, *Journal of Hydrology*, 518,
700 250–266, <https://doi.org/https://doi.org/10.1016/j.jhydrol.2013.06.037>, 2014.
- Koch, J., Demirel, M. C., and Stisen, S.: The SPATial Efficiency metric (SPAEF): Multiple-component evaluation of spatial patterns for optimization of hydrological models, *Geoscientific Model Development*, 11, 1873–1886, <https://doi.org/10.5194/gmd-11-1873-2018>, 2018.
- Koivusalo, H. and Kokkonen, T.: Snow processes in a forest clearing and in a coniferous forest, *Journal of Hydrology*, 262, 145–164, [https://doi.org/10.1016/S0022-1694\(02\)00031-8](https://doi.org/10.1016/S0022-1694(02)00031-8), 2002.
- 705 Kolari, P., Lappalainen, H. K., Hänninen, H., and Hari, P.: Relationship between temperature and the seasonal course of photosynthesis in Scots pine at northern timberline and in southern boreal zone, *Tellus, Series B: Chemical and Physical Meteorology*, 59, 542–552, <https://doi.org/10.1111/j.1600-0889.2007.00262.x>, 2007.
- Kollet, S. J. and Maxwell, R. M.: Capturing the influence of groundwater dynamics on land surface processes using an integrated, distributed watershed model, *Water Resources Research*, 44, 1–18, <https://doi.org/10.1029/2007WR006004>, 2008.
- 710 Korkiakoski, M., Määttä, T., Peltoniemi, K., Penttilä, T., and Lohila, A.: Excess soil moisture and fresh carbon input are prerequisites for methane production in podzolic soil, *Biogeosciences*, 19, 2025–2041, <https://doi.org/10.5194/bg-19-2025-2022>, 2022.
- Kozii, N., Haahti, K., Tor-Ngern, P., Chi, J., Maher Hasselquist, E., Laudon, H., Launiainen, S., Oren, R., Peichl, M., Wallerman, J. r., and Hasselquist, N. J.: Partitioning growing season water balance within a forested boreal catchment using sap flux, eddy covariance, and a process-based model, *Hydrology and Earth System Sciences*, 24, 2999–3014, <https://doi.org/10.5194/hess-24-2999-2020>, 2020.
- 715 Krinner, G.: Impact of lakes and wetlands on boreal climate, *Journal of Geophysical Research: Atmospheres*, 108, <https://doi.org/10.1029/2002jd002597>, 2003.
- Kuusisto, E.: Snow accumulation and snowmelt in Finland, *PUBLICATIONS OF THE WATER RESEARCH INSTITUTE*, 55 edn., 1984.

- Lagergren, F. and Lindroth, A.: Transpiration response to soil moisture in pine and spruce trees in Sweden, *Agricultural and Forest Meteorology*, 112, 67–85, [https://doi.org/10.1016/S0168-1923\(02\)00060-6](https://doi.org/10.1016/S0168-1923(02)00060-6), 2002.
- 720 Larson, J., Wallerman, J., Peichl, M., and Laudon, H.: Soil moisture controls the partitioning of carbon stocks across a managed boreal forest landscape., *Scientific reports*, 13, 14 909, <https://doi.org/10.1038/s41598-023-42091-4>, 2023.
- Launiainen, S., Katul, G. G., Lauren, A., and Kolari, P.: Coupling boreal forest CO₂, H₂O and energy flows by a vertically structured forest canopy - Soil model with separate bryophyte layer, *Ecological Modelling*, 312, 385–405, <https://doi.org/10.1016/j.ecolmodel.2015.06.007>, 2015.
- 725 Launiainen, S., Katul, G. G., Kolari, P., Lindroth, A., Lohila, A., Aurela, M., Varlagin, A., Grelle, A., and Vesala, T.: Do the energy fluxes and surface conductance of boreal coniferous forests in Europe scale with leaf area?, *Global Change Biology*, 22, 4096–4113, <https://doi.org/10.1111/gcb.13497>, 2016.
- Launiainen, S., Guan, M., Salmivaara, A., and Kieloaho, A. J.: Modeling boreal forest evapotranspiration and water balance at stand and catchment scales: a spatial approach, *Hydrology and Earth System Sciences*, 23, 3457–3480, <https://doi.org/10.5194/hess-23-3457-2019>,
730 2019.
- Launiainen, S., Kieloaho, A. J., Lindroos, A. J., Salmivaara, A., Ilvesniemi, H., and Heiskanen, J.: Water Retention Characteristics of Mineral Forest Soils in Finland: Impacts for Modeling Soil Moisture, *Forests*, 13, <https://doi.org/10.3390/f13111797>, 2022.
- Laurén, A., Palviainen, M., Launiainen, S., Leppä, K., Stenberg, L., Urzainki, I., Nieminen, M., Laiho, R., and Hökkä, H.: Drainage and stand growth response in peatland forests—description, testing, and application of mechanistic peatland simulator susi, *Forests*, 12, 1–23, <https://doi.org/10.3390/f12030293>, 2021.
- 735 Lawrence, D. M., Oleson, K. W., Flanner, M. G., Fletcher, C. G., Lawrence, P. J., Levis, S., Swenson, S. C., and Bonan, G. B.: The CCSM4 Land Simulation, 1850–2005: Assessment of Surface Climate and New Capabilities, *Journal of Climate*, 25, 2240–2260, <https://doi.org/https://doi.org/10.1175/JCLI-D-11-00103.1>, 2012.
- Leppä, K., Hökkä, H., Laiho, R., Launiainen, S., Lehtonen, A., Mäkipää, R., Peltoniemi, M., Saarinen, M., Sarkkola, S., and Nieminen, M.: Selection Cuttings as a Tool to Control Water Table Level in Boreal Drained Peatland Forests, *Frontiers in Earth Science*, 8, 1–16, <https://doi.org/10.3389/feart.2020.576510>, 2020.
- 740 Li, F., Kurtz, W., Hung, C. P., Vereecken, H., and Hendricks Franssen, H. J.: Water table depth assimilation in integrated terrestrial system models at the larger catchment scale, *Frontiers in Water*, 5, <https://doi.org/10.3389/frwa.2023.1150999>, 2023.
- Li, M., Wu, P., Ma, Z., Lv, M., Yang, Q., and Duan, Y.: The decline in the groundwater table depth over the past four decades in China simulated by the Noah-MP land model, *Journal of Hydrology*, 607, 127 551, <https://doi.org/https://doi.org/10.1016/j.jhydrol.2022.127551>,
745 2022.
- Lin, Y. S., Medlyn, B. E., Duursma, R. A., Prentice, I. C., Wang, H., Baig, S., Eamus, D., De Dios, V. R., Mitchell, P., Ellsworth, D. S., De Beeck, M. O., Wallin, G., Uddling, J., Tarvainen, L., Linderson, M. L., Cernusak, L. A., Nippert, J. B., Ocheltree, T. W., Tissue, D. T., Martin-StPaul, N. K., Rogers, A., Warren, J. M., De Angelis, P., Hikosaka, K., Han, Q., Onoda, Y., Gimeno, T. E., Barton, C. V.,
750 Bennie, J., Bonal, D., Bosc, A., Löw, M., Macinins-Ng, C., Rey, A., Rowland, L., Setterfield, S. A., Tausz-Posch, S., Zaragoza-Castells, J., Broadmeadow, M. S., Drake, J. E., Freeman, M., Ghannoum, O., Hutley, L. B., Kelly, J. W., Kikuzawa, K., Kolari, P., Koyama, K., Limousin, J. M., Meir, P., Da Costa, A. C., Mikkelsen, T. N., Salinas, N., Sun, W., and Wingate, L.: Optimal stomatal behaviour around the world, *Nature Climate Change*, 5, 459–464, <https://doi.org/10.1038/nclimate2550>, 2015.
- Lindsay, J. B.: The Whitebox Geospatial Analysis Tools project and open-access GIS, *Proceedings of the GIS research UK 22nd annual conference*, 2014.
755

- Liu, J., Engel, B. A., Wang, Y., Wu, Y., Zhang, Z., and Zhang, M.: Runoff Response to Soil Moisture and Micro-topographic Structure on the Plot Scale, *Scientific Reports*, 9, 1–13, <https://doi.org/10.1038/s41598-019-39409-6>, 2019.
- Lohila, A., Penttilä, T., Jortikka, S., Aalto, T., Anttila, P., Asmi, E., Aurela, M., Hatakka, J., Hellén, H., Henttonen, H., Hänninen, P., Kilkki, J., Kyllönen, K., Laurila, T., Lepistö, A., Lihavainen, H., Makkonen, U., Paatero, J., Rask, M., Sutinen, R., Tuovinen, J. P., Vuorenmaa, J., and Viisanen, Y.: Preface to the special issue on integrated research of atmosphere, ecosystems and environment at Pallas, *Boreal Environment Research*, 20, 431–454, 2015.
- Lohila, A., Aalto, T., Aurela, M., Hatakka, J., Tuovinen, J. P., Kilkki, J., Penttilä, T., Vuorenmaa, J., Hänninen, P., Sutinen, R., Viisanen, Y., and Laurila, T.: Large contribution of boreal upland forest soils to a catchment-scale CH₄ balance in a wet year, *Geophysical Research Letters*, 43, 2946–2953, <https://doi.org/10.1002/2016GL067718>, 2016.
- 765 Ma, L., He, C., Bian, H., and Sheng, L.: MIKE SHE modeling of ecohydrological processes: Merits, applications, and challenges, *Ecological Engineering*, 96, 137–149, <https://doi.org/10.1016/j.ecoleng.2016.01.008>, 2016.
- Makhnykina, A. V., Prokushkin, A. S., Menyailo, O. V., Verkhovets, S. V., Tychkov, I. I., Urban, A. V., Rubtsov, A. V., Koshurnikova, N. N., and Vaganov, E. A.: The Impact of Climatic Factors on C₂ Emissions from Soils of Middle-Taiga Forests in Central Siberia: Emission as a Function of Soil Temperature and Moisture, *Russian Journal of Ecology*, 51, 46–56, <https://doi.org/10.1134/S1067413620010063>, 2020.
- 770 Mäkisara, K., Katila, M., Peräsaari, J., and Tomppo, E.: The Multi-source National Forest Inventory of Finland – methods and results 2013. Natural resources and bioeconomy studies 10/2016, *Natural resources and bioeconomy studies*, p. 224, <http://urn.fi/URN:ISBN:978-952-326-186-0>, 2016.
- Maneta, M. P. and Silverman, N. L.: A spatially distributed model to simulate water, energy, and vegetation dynamics using information from regional climate models, *Earth Interactions*, 17, <https://doi.org/10.1175/2012EI000472.1>, 2013.
- 775 Manninen, T., Jaaskelainen, E., Lohila, A., Korkiakoski, M., Rasanen, A., Virtanen, T., Muhic, F., Marttila, H., Ala-Aho, P., Markovaara-Koivisto, M., Liwata-Kenttala, P., Sutinen, R., and Hanninen, P.: Very High Spatial Resolution Soil Moisture Observation of Heterogeneous Subarctic Catchment Using Nonlocal Averaging and Multitemporal SAR Data, *IEEE Transactions on Geoscience and Remote Sensing*, pp. 1–17, <https://doi.org/10.1109/TGRS.2021.3109695>, 2021.
- Marttila, H., Lohila, A., Ala-Aho, P., Noor, K., Welker, J. M., Croghan, D., Mustonen, K., Meriö, L., Autio, A., Muhic, F., Bailey, H., Aurela, M., Vuorenmaa, J., Penttilä, T., Hyöky, V., Klein, E., Kuzmin, A., Korpelainen, P., Kumpula, T., Rauhala, A., and Kløve, B.: Subarctic catchment water storage and carbon cycling – Leading the way for future studies using integrated datasets at Pallas, Finland, *Hydrological Processes*, 35, 1–19, <https://doi.org/10.1002/hyp.14350>, 2021.
- 780 Mathijssen, P., Tuovinen, J.-P., Lohila, A., Aurela, M., Juutinen, S., Laurila, T., Niemelä, E., Tuittila, E.-S., and Välranta, M.: Development, carbon accumulation, and radiative forcing of a subarctic fen over the Holocene, *The Holocene*, 24, 1156–1166, <https://doi.org/10.1177/0959683614538072>, 2014.
- 785 Maxwell, R. M. and Condon, L. E.: Connections between groundwater flow and transpiration partitioning, *Science*, 353, 377–380, <https://doi.org/10.1126/science.aaf7891>, 2016.
- Maxwell, R. M., Chow, F. K., and Kollet, S. J.: The groundwater-land-surface-atmosphere connection: Soil moisture effects on the atmospheric boundary layer in fully-coupled simulations, *Advances in Water Resources*, 30, 2447–2466, <https://doi.org/10.1016/j.advwatres.2007.05.018>, 2007.
- 790 Mazzotti, G., Webster, C., Essery, R., and Jonas, T.: Increasing the Physical Representation of Forest-Snow Processes in Coarse-Resolution Models: Lessons Learned From Upscaling Hyper-Resolution Simulations, *Water Resources Research*, 57, 1–21, <https://doi.org/10.1029/2020WR029064>, 2021.

- Menberu, M. W., Marttila, H., Ronkanen, A., Haghghi, A. T., and Kløve, B.: Hydraulic and Physical Properties of Managed
795 and Intact Peatlands: Application of the Van Genuchten-Mualem Models to Peat Soils, *Water Resources Research*, 57, 1–22,
<https://doi.org/10.1029/2020wr028624>, 2021.
- Meriö, L.-J., Rauhala, A., Ala-aho, P., Kuzmin, A., Korpelainen, P., Kumpula, T., Kløve, B., and Marttila, H.: Measuring the spatiotemporal
variability of snow depth in subarctic environments using unmanned aircraft systems (UAS) – Part 2: Snow processes and snow-canopy
interactions, *The Cryosphere Discussions*, 2023, 1–28, <https://doi.org/10.5194/tc-2022-242>, 2023.
- 800 Miguez-Macho, G., Fan, Y., Weaver, C. P., Walko, R., and Robock, A.: Incorporating water table dynamics in climate mod-
eling: 2. Formulation, validation, and soil moisture simulation, *Journal of Geophysical Research Atmospheres*, 112, 1–16,
<https://doi.org/10.1029/2006JD008112>, 2007.
- Moges, E., Demissie, Y., Larsen, L., and Yassin, F.: Review: Sources of Hydrological Model Uncertainties and Advances in Their Analysis,
<https://doi.org/10.3390/w13010028>, 2021.
- 805 Moreno, J., Asensio, S., Berdugo, M., Gozalo, B., Ochoa, V., Pescador, D. S., Benito, B. M., and Maestre, F. T.: Fourteen years of continuous
soil moisture records from plant and biocrust-dominated microsites, *Scientific Data*, 9, 1–7, <https://doi.org/10.1038/s41597-021-01111-6>,
2022.
- Muukkonen, P., Nevalainen, S., Lindgren, M., and Peltoniemi, M.: Spatial occurrence of drought-associated damages in Finnish boreal
forests: Results from forest condition monitoring and GIS analysis, *Boreal Environment Research*, 20, 172–180, 2015.
- 810 Nakhavali, M., Lauerwald, R., Regnier, P., Guenet, B., Chadburn, S., and Friedlingstein, P.: Leaching of dissolved organic car-
bon from mineral soils plays a significant role in the terrestrial carbon balance, *Global Change Biology*, 27, 1083–1096,
<https://doi.org/https://doi.org/10.1111/gcb.15460>, 2021.
- Niu, G. Y., Yang, Z. L., Mitchell, K. E., Chen, F., Ek, M. B., Barlage, M., Kumar, A., Manning, K., Niyogi, D., Rosero, E., Tewari, M., and
Xia, Y.: The community Noah land surface model with multiparameterization options (Noah-MP): 1. Model description and evaluation
815 with local-scale measurements, *Journal of Geophysical Research Atmospheres*, 116, 1–19, <https://doi.org/10.1029/2010JD015139>, 2011.
- Niu, G. Y., Paniconi, C., Troch, P. A., Scott, R. L., Durcik, M., Zeng, X., Huxman, T., and Goodrich, D. C.: An integrated modelling
framework of catchment-scale ecohydrological processes: 1. Model description and tests over an energy-limited watershed, *Ecohydrology*,
7, 427–439, <https://doi.org/10.1002/eco.1362>, 2014.
- Niu, Z., He, H., Peng, S., Ren, X., Zhang, L., Gu, F., Zhu, G., Peng, C., Li, P., Wang, J., Ge, R., Zeng, N., Zhu, X., Lv, Y., Chang, Q., Xu,
820 Q., Zhang, M., and Liu, W.: A Process-Based Model Integrating Remote Sensing Data for Evaluating Ecosystem Services, *Journal of
Advances in Modeling Earth Systems*, 13, e2020MS002451, <https://doi.org/https://doi.org/10.1029/2020MS002451>, 2021.
- NLSF: National Land Survey of Finland Topographic Database, available at: [http://www.maanmittauslaitos.fi/en/e-services/open-data-file-
download-service](http://www.maanmittauslaitos.fi/en/e-services/open-data-file-download-service), 2020.
- Noilhan, J. and Mahfouf, J. F.: The ISBA land surface parameterisation scheme, *Global and Planetary Change*, 13, 145–159,
825 [https://doi.org/10.1016/0921-8181\(95\)00043-7](https://doi.org/10.1016/0921-8181(95)00043-7), 1996.
- Nolan, M. and Fatland, D. R.: Penetration depth as a DInSAR observable and proxy for soil moisture, *IEEE Transactions on Geoscience and
Remote Sensing*, 41, 532–537, <https://doi.org/10.1109/TGRS.2003.809931>, 2003.
- Nousu, J.-P., Lafaysse, M., Mazzotti, G., Ala-aho, P., Marttila, H., Cluzet, B., Aurela, M., Lohila, A., Kolari, P., Boone, A., Fructus, M.,
and Launiainen, S.: Modelling snowpack dynamics and surface energy budget in boreal and subarctic peatlands and forests, *EGUphere*,
830 2023, 1–52, <https://doi.org/10.5194/egusphere-2023-338>, 2023.
- Nousu, J.-P., Leppä, K., and Launiainen, S.: LukeEcomod/SpaFHY_v1_Pallas_2D, <https://doi.org/10.5281/zenodo.10820456>, 2024a.

- Nousu, J.-P., Leppä, K., Marttila, H., Ala-Aho, P., Mazzotti, G., Manninen, T., Korkiakoski, M., Aurela, M., Lohila, A., and Launiainen, S.: Multi-scale soil moisture data and process-based modeling reveal the importance of lateral groundwater flow in a subarctic catchment, <https://doi.org/10.5281/zenodo.10820563>, 2024b.
- 835 O'Callaghan, J. F. and Mark, D. M.: The extraction of drainage networks from digital elevation data, *Computer Vision, Graphics, and Image Processing*, 28, 323–344, [https://doi.org/10.1016/S0734-189X\(84\)80011-0](https://doi.org/10.1016/S0734-189X(84)80011-0), 1984.
- Olson, D. M., Dinerstein, E., Wikramanayake, E. D., Burgess, N. D., Powell, G. V., Underwood, E. C., D'Amico, J. A., Itoua, I., Strand, H. E., Morrison, J. C., Loucks, C. J., Allnutt, T. F., Ricketts, T. H., Kura, Y., Lamoreux, J. F., Wettengel, W. W., Hedao, P., and Kassem, K. R.: Terrestrial ecoregions of the world: A new map of life on Earth, *BioScience*, 51, 933–938, [https://doi.org/10.1641/0006-8403568\(2001\)051\[0933:TEOTWA\]2.0.CO;2](https://doi.org/10.1641/0006-8403568(2001)051[0933:TEOTWA]2.0.CO;2), 2001.
- Panday, S. and Huyakorn, P. S.: A fully coupled physically-based spatially-distributed model for evaluating surface/subsurface flow, *Advances in Water Resources*, 27, 361–382, <https://doi.org/10.1016/j.advwatres.2004.02.016>, 2004.
- Pomeroy, J. W., Parviainen, J., Hedstrom, N., and Gray, D. M.: Coupled modelling of forest snow interception and sublimation, *Hydrological Processes*, 12, 2317–2337, [https://doi.org/10.1002/\(SICI\)1099-1085\(199812\)12:15<2317::AID-HYP799>3.0.CO;2-X](https://doi.org/10.1002/(SICI)1099-1085(199812)12:15<2317::AID-HYP799>3.0.CO;2-X), 1998.
- 845 Quast, R., Wagner, W., Bauer-Marschallinger, B., and Vreugdenhil, M.: Soil moisture retrieval from Sentinel-1 using a first-order radiative transfer model—A case-study over the Po-Valley, *Remote Sensing of Environment*, 295, 113 651, <https://doi.org/https://doi.org/10.1016/j.rse.2023.113651>, 2023.
- Räsänen, J.: Snow conditions in northern Europe: The dynamics of interannual variability versus projected long-term change, *Cryosphere*, 15, 1677–1696, <https://doi.org/10.5194/tc-15-1677-2021>, 2021.
- 850 Raleigh, M. S., Lundquist, J. D., and Clark, M. P.: Exploring the impact of forcing error characteristics on physically based snow simulations within a global sensitivity analysis framework, *Hydrology and Earth System Sciences*, 19, 3153–3179, <https://doi.org/10.5194/hess-19-3153-2015>, 2015.
- Räsänen, A., Manninen, T., Korkiakoski, M., Lohila, A., and Virtanen, T.: Predicting catchment-scale methane fluxes with multi-source remote sensing, *Landscape Ecology*, 36, 1177–1195, <https://doi.org/10.1007/s10980-021-01194-x>, 2021.
- 855 Räsänen, A., Tolvanen, A., and Kareksela, S.: Monitoring peatland water table depth with optical and radar satellite imagery, *International Journal of Applied Earth Observation and Geoinformation*, 112, 102 866, <https://doi.org/https://doi.org/10.1016/j.jag.2022.102866>, 2022.
- Robinson, D., Campbell, C., Hopmans, J., Hornbuckle, B., Jones, S., Knight, R., Ogden, F., Selker, J., and Wendroth, O.: Soil Moisture Measurement for Ecological and Hydrological Watershed-Scale Observatories: A Review All rights reserved. No part of this periodical may be reproduced or transmitted in any form or by any means, electronic or mechanical, including photocopyin, *Vadose Zone J.*, 7, 860 358–389, 2008.
- Ruosteenoja, K., Markkanen, T., Venäläinen, A., Räsänen, P., and Peltola, H.: Seasonal soil moisture and drought occurrence in Europe in CMIP5 projections for the 21st century, *Climate Dynamics*, 50, 1177–1192, <https://doi.org/10.1007/s00382-017-3671-4>, 2018.
- Salmivaara, A., Launiainen, S., Perttunen, J., Nevalainen, P., Pohjankukka, J., Ala-Ilomäki, J., Sirén, M., Laurén, A., Tuominen, S., Uusitalo, J., Pahikkala, T., Heikkonen, J., and Finér, L.: Towards dynamic forest trafficability prediction using open spatial data, hydrological modelling and sensor technology, *Forestry*, 93, 662–674, <https://doi.org/10.1093/FORESTRY/CPAA010>, 2021.
- 865 Schneider, J., Jungkunst, H. F., Wolf, U., Schreiber, P., Gazovic, M., Miglovetz, M., Mikhaylov, O., Grunwald, D., Erasmí, S., Wilmking, M., and Kutzbach, L.: Russian boreal peatlands dominate the natural European methane budget, *Environmental Research Letters*, 11, <https://doi.org/10.1088/1748-9326/11/1/014004>, 2016.

- Seibert, J. and Vis, M. J. P.: Teaching hydrological modeling with a user-friendly catchment-runoff-model software package, *Hydrology and Earth System Sciences*, 16, 3315–3325, <https://doi.org/10.5194/hess-16-3315-2012>, 2012.
- 870 Seneviratne, S. I., Corti, T., Davin, E. L., Hirschi, M., Jaeger, E. B., Lehner, I., Orlowsky, B., and Teuling, A. J.: Investigating soil moisture-climate interactions in a changing climate: A review, *Earth-Science Reviews*, 99, 125–161, <https://doi.org/10.1016/j.earscirev.2010.02.004>, 2010.
- Shellito, P. J., Kumar, S. V., Santanello, J. A., Lawston-Parker, P., Bolten, J. D., Cosh, M. H., Bosch, D. D., Collins, C. D. H., Livingston, S., Prueger, J., Seyfried, M., and Starks, P. J.: Assessing the Impact of Soil Layer Depth Specification on the Observability of Modeled Soil Moisture and Brightness Temperature, *Journal of Hydrometeorology*, 21, 2041 – 2060, <https://doi.org/10.1175/JHM-D-19-0280.1>, 2020.
- 875 Sidle, R. C.: Strategies for smarter catchment hydrology models: incorporating scaling and better process representation, *Geoscience Letters*, 8, <https://doi.org/10.1186/s40562-021-00193-9>, 2021.
- Singh, N. K., Emanuel, R. E., McGlynn, B. L., and Miniati, C. F.: Soil Moisture Responses to Rainfall: Implications for Runoff Generation, *Water Resources Research*, 57, e2020WR028 827, <https://doi.org/https://doi.org/10.1029/2020WR028827>, 2021.
- 880 Skaggs, R. W.: A Water Management Model for Artificially Drained Soils, North Carolina Agri. Exp. Station Tech. Bul, North Carolina Agricultural Research Service, <https://books.google.fi/books?id=F3JRAQAAMAAJ>, 1980.
- Skofronick-Jackson, G., Petersen, W. A., Berg, W., Kidd, C., Stocker, E. F., Kirschbaum, D. B., Kakar, R., Braun, S. A., Huffman, G. J., Iguchi, T., Kirstetter, P. E., Kummerow, C., Meneghini, R., Oki, R., Olson, W. S., Takayabu, Y. N., Furukawa, K., and Wilhelm, T.: The Global Precipitation Measurement (GPM) Mission for Science and Society, *Bulletin of the American Meteorological Society*, 98, 1679 – 1695, <https://doi.org/10.1175/BAMS-D-15-00306.1>, 2017.
- 885 Smith, B., Prentice, I. C., and Sykes, M. T.: Representation of vegetation dynamics in the modelling of terrestrial ecosystems: comparing two contrasting approaches within European climate space, *Global Ecology and Biogeography*, 10, 621–637, <https://doi.org/https://doi.org/10.1046/j.1466-822X.2001.t01-1-00256.x>, 2001.
- 890 Stenberg, L., Leppä, K., Launiainen, S., Laurén, A., Hökkä, H., Sarkkola, S., Saarinen, M., and Nieminen, M.: Measuring and Modeling the Effect of Strip Cutting on the Water Table in Boreal Drained Peatland Pine Forests, *Forests*, 13, <https://doi.org/10.3390/f13071134>, 2022.
- Stuefer, S. L., Kane, D. L., and Dean, K. M.: Snow Water Equivalent Measurements in Remote Arctic Alaska Watersheds, *Water Resources Research*, 56, 1–12, <https://doi.org/10.1029/2019WR025621>, 2020.
- 895 Tang, J., Pilesjö, P., Miller, P. A., Persson, A., Yang, Z., Hanna, E., and Callaghan, T. V.: Incorporating topographic indices into dynamic ecosystem modelling using LPJ-GUESS, *Ecohydrology*, 7, 1147–1162, <https://doi.org/https://doi.org/10.1002/eco.1446>, 2014.
- Thornton, J. M., Therrien, R., Mariéthoz, G., Linde, N., and Brunner, P.: Simulating Fully-Integrated Hydrological Dynamics in Complex Alpine Headwaters: Potential and Challenges, *Water Resources Research*, 58, <https://doi.org/10.1029/2020WR029390>, 2022.
- 900 Toca, L., Artz, R. R. E., Smart, C., Quaife, T., Morrison, K., Gimona, A., Hughes, R., Hancock, M. H., and Klein, D.: Potential for Peatland Water Table Depth Monitoring Using Sentinel-1 SAR Backscatter: Case Study of Forsinard Flows, Scotland, UK, <https://doi.org/10.3390/rs15071900>, 2023.
- Tyystjärvi, V., Kempainen, J., Luoto, M., Aalto, T., Markkanen, T., Launiainen, S., Kieloaho, A. J., and Aalto, J.: Modelling spatio-temporal soil moisture dynamics in mountain tundra, *Hydrological Processes*, 36, <https://doi.org/10.1002/hyp.14450>, 2022.
- van Genuchten, M. T.: A Closed-form Equation for Predicting the Hydraulic Conductivity of Unsaturated Soils, *Soil Science Society of America Journal*, 44, 892–898, <https://doi.org/10.2136/sssaj1980.03615995004400050002x>, 1980.

- 905 Venäläinen, A., Lehtonen, I., Laapas, M., Ruosteenoja, K., Tikkanen, O.-P., Viiri, H., Ikonen, V.-P., and Peltola, H.: Climate change induces multiple risks to boreal forests and forestry in Finland: A literature review, *Global Change Biology*, 26, 4178–4196, <https://doi.org/https://doi.org/10.1111/gcb.15183>, 2020.
- Wang, T., Zhang, H., Zhao, J., Wu, R., Li, H., Guo, X., and Zhao, H.: Increased atmospheric moisture demand induced a reduction in the water content of boreal forest during the past three decades, *Agricultural and Forest Meteorology*, 342, 109 759, 910 <https://doi.org/10.1016/j.agrformet.2023.109759>, 2023.
- Webster, C., Essery, R., Mazzotti, G., and Jonas, T.: Using just a canopy height model to obtain lidar-level accuracy in 3D forest canopy shortwave transmissivity estimates, *Agricultural and Forest Meteorology*, 338, 109 429, <https://doi.org/10.1016/j.agrformet.2023.109429>, 2023.
- Williams, T. G. and Flanagan, L. B.: Effect of changes in water content on photosynthesis, transpiration and discrimination against ^{13}C and $\text{C}^{18}\text{O}^{16}\text{O}$ in *Pleurozium* and *Sphagnum*, *Oecologia*, 108, 38–46, <https://doi.org/10.1007/BF00333212>, 1996.
- 915 Wood, E. F., Roundy, J. K., Troy, T. J., van Beek, L. P. H., Bierkens, M. F. P., Blyth, E., de Roo, A., Döll, P., Ek, M., Famiglietti, J., Gochis, D., van de Giesen, N., Houser, P., Jaffé, P. R., Kollet, S., Lehner, B., Lettenmaier, D. P., Peters-Lidard, C., Sivapalan, M., Sheffield, J., Wade, A., and Whitehead, P.: Hyperresolution global land surface modeling: Meeting a grand challenge for monitoring Earth’s terrestrial water, *Water Resources Research*, 47, <https://doi.org/https://doi.org/10.1029/2010WR010090>, 2011.
- 920 Yu, L., Gao, W., Shamshiri, R. R., Tao, S., Ren, Y., Zhang, Y., and Su, G.: Review of research progress on soil moisture sensor technology, *International Journal of Agricultural and Biological Engineering*, 14, 32–42, <https://doi.org/10.25165/j.ijabe.20211404.6404>, 2021.
- Yu, S., Lu, F., Zhou, Y., Wang, X., Wang, K., Song, X., and Zhang, M.: Evaluation of Three High-Resolution Remote Sensing Precipitation Products on the Tibetan Plateau, <https://doi.org/10.3390/w14142169>, 2022.
- Zeng, Y., Xie, Z., Liu, S., Xie, J., Jia, B., Qin, P., and Gao, J.: Global Land Surface Modeling Including Lateral Groundwater Flow, *Journal of Advances in Modeling Earth Systems*, 10, 1882–1900, <https://doi.org/https://doi.org/10.1029/2018MS001304>, 2018.
- 925 Zhang, F. and Zhou, G.: Estimation of Canopy Water Content by Means of Hyperspectral Indices Based on Drought Stress Gradient Experiments of Maize in the North Plain China, <https://doi.org/10.3390/rs71115203>, 2015.
- Zhang, H., Liu, J., Li, H., Meng, X., and Ablikim, A.: The Impacts of Soil Moisture Initialization on the Forecasts of Weather Research and Forecasting Model: A Case Study in Xinjiang, China, <https://doi.org/10.3390/w12071892>, 2020a.
- 930 Zhang, H., Tuittila, E. S., Korrensalo, A., Räsänen, A., Virtanen, T., Aurela, M., Penttilä, T., Laurila, T., Gerin, S., Lindholm, V., and Lohila, A.: Water flow controls the spatial variability of methane emissions in a northern valley fen ecosystem, *Biogeosciences*, 17, 6247–6270, <https://doi.org/10.5194/bg-17-6247-2020>, 2020b.
- Zhang, Y., Gong, J., Sun, K., Yin, J., and Chen, X.: Estimation of soil moisture index using multi-temporal Sentinel-1 images over Poyang Lake ungauged zone, *Remote Sensing*, 10, 1–19, <https://doi.org/10.3390/rs10010012>, 2018.